People's Democratic Republic of Algeria

Ministry of Higher Education and Scientific Research

University M'Hamed BOUGARA – Boumerdes

Institute of Electrical and Electronic Engineering

Department of Electronics

Final Year Project Report Presented in Partial Fulfillment of the Requirements for the Degree of

MASTER

In **Telecommunication**

Option: **Telecommunications**

Title:

Design and Implementation of Microstrip Ultra-Wide Band Bandpass Filter with and without Dual Notched Band

Presented by:

- **ALIOUANE Mohamed Abdelbasset**
- **SKOUDARLI Abdelhamid**

Supervisor:

Prof. M. CHALLAL

Registration Number:……/2019

Abstract

This work presents a novel compact ultra-wideband bandpass filter (UWB BPF) with and without dual notched band. It is based on symmetrical structure of a simple uniform line loaded by a stepped-impedance stub (SIS) connected at its center. Two notches are inserted at 5.8 and 8.0 GHz to eliminate WiMAX and satellite communication interferences by embedding two U-shaped slots in the ground plane. The proposed UWB BPF with dual-notch is simulated, fabricated and measured. Satisfactory results are obtained, achieving good performances in terms of ultra-wide impedance bandwidth of 7.7 GHz (2.9 - 10.6 GHz) with a fractional bandwidth of 118.8 %, return loss better than 13 dB, an upper stopband attenuation higher than 20 dB up to 16 GHz, and a sharp selectivity.

Keywords: Ultra-wideband (UWB), bandpass filter (BPF), stepped-impedance stub (SIS), Notches, WiMAX and satellite communication interferences.

ACKNOWLEDGEMENT

First and foremost, we are thankful to Allah, the most gracious, the most merciful for helping us to finish this modest work. It is our belief in him that helped us persevere at times when it seemed impossible to go on.

Secondly, we would like to express our deepest gratitude to our supervisor Prof. M. CHALLAL for his help and guidance during the realization of this project. It has been an absolute privilege working with him.

Also, we take this opportunity to express our deep and special thanks to Dr. A. TAIBI and Dr. F. MOUHOUCHE for their continuing technical support in the implementation of our project and their valuable support throughout this work.

Finally, we would like to thank our family, friends and all IGEE teachers for their support and encouragement.

Dedication

We dedicate this work to our beloved parents, who have been our source of inspiration and gave us strength when we thought of giving up, who continually provide their moral, spiritual, emotional, and financial support. To our brothers, sisters, relatives, mentor, friends, and classmates who shared their words of advice and encouragement to finish this work.

Table of Content

CHAPTER II: Theory of Filters and UWB Technology

List of Tables

List of Figures

List of Abbreviations

ADS	Advanced Design System
BPF	Band Pass Filter
BW	Bandwidth
CDMA	Code Division Multiple Access
CSRR	Complementary Split Ring Resonator
CST	Computer Simulation Technology
DGS	Defected Ground Structure
FBW	Fractional Bandwidth
FCC	Federal Communications Commission
FR4	Flame Retardant 4
GPS	Global Positioning System
GSM	Global System for Mobile communication
HPF	High Pass Filter
IEEE	Institute of Electrical and Electronic Engineers
ITT	International Telephone and Telegraph
LPF	Low Pass Filter
MMR	Multiple-Mode Resonators
RF	Radio Frequency
RFID	Radio Frequency Identification
SIR	Stepped Impedance Resonator
SIS	Stepped Impedance Stub
SRR	Split Ring Resonator
TE	Transverse Electric
TEM	Transverse Electromagnetic
TM	Transverse Magnetic
UWB	Ultra-Wide Band
VNA	Vector Network Analyzer
Wi-Fi	Wireless Fidelity
WiMAX	Worldwide Interoperability for Microwave Access.
WLAN	Wireless Local Area Network

List of Symbols

W	Strip line width
t	Strip line thickness
h	Substrate thickness
$\boldsymbol{\lambda_g}$	Guided wavelength
$\boldsymbol{\beta}$	Propagation constant
$\boldsymbol{v_p}$	Phase velocity
$\boldsymbol{\theta}$	Electrical length
Q	Quality factor
c	Light velocity
$\boldsymbol{\varepsilon_{eff}}$	Effective dielectric constant
$\boldsymbol{\varepsilon_r}$	Relative Permittivity
C	Capacitance
L	Inductance
R	Resistance
Z	Impedance
$\mathbf{Z_0}$	Characteristic Impedance
Y	Admittance
$\mathbf{Y_0}$	Characteristic admittance
E	Electric Field
H	Magnetic Field
f	Operating frequency
$\mathbf{f_0}$	Center frequency
$\mathbf{f_c}$	Cutoff frequency
$\mathbf{S_{ij}}$	Scattering parameters
m	Meter
s	Second
Hz	Hertz
dB	Decibel
H	Henry
F	Farad

General Introduction

Effective communication between two distance places has always been a challenge for the human race. From the use of flags, color codes, reflecting surface to telegraph, wireless devices and communication satellites, human race has come a long way. However, the quest for precise and affordable communication has not diminished. With the advent of the information era, numerous advanced communication technologies have arisen during the past two decades which, have greatly influenced and benefited every field of human society. In countless homes and offices, the cordless phones free us from the short leash of handset cords. Cell phones give us even more freedom such that we can communicate with each other at any time and in any place [1].

In wireless systems, RF filters are considered one of the most important components. These filters are used to filter/ prevent unwanted signals from accessing a system. They play an extremely important role in minimizing interferences from undesired signals, especially with the increase of wireless standards in the existing frequency bands. There exists a number of filter types such as: Notch Filters, Cavity Filters and Waveguide Filters that are designed based on the required application and size of the wireless system. Each type has its own form factors and properties [2].

Future wireless devices will be expected to communicate over several bands with various other devices in order to fine tune the services they provide to the user. Each band may require a separate RF transceiver and such modern wireless multi-band multi-mode communication systems call for high performance, highly integrated compact modules. Since the Federal Communications Commission (FCC) released the unlicensed frequency band 3.1-10.6 GHz for ultra-wideband (UWB) commercial communications, the development race for commercializing UWB technology has seen a dramatic increase around the world [3].

In this work, a compact Microstrip UWB BPF based on stepped impedance stub (SIS) which provides (2.9 – 10.6 GHz) passband is proposed. A dual notched band to eliminate WiMAX and satellite communication interferences are created at 5.8 GHz and 8.0 GHz respectively. The filter is designed, analyzed and implemented using FR4 substrate material with relative dielectric constant of 4.3, a thickness of 1.62 mm, a copper thickness 0.035 mm and a loss tangent of 0.017. The design and simulations are carried out using ADS and CST software.

This report contains three chapters organized as follows:

Chapter I: reviews basic concepts of RF and Microwave theories, and provides literature review of Microstrip technology.

Chapter II: defines theory of filters and introduces Ultra-Wide Band (UWB) technology; its applications, advantages and disadvantages.

Chapter III: represents the analysis, design, simulation, and implementation of the proposed UWB BPF with and without dual notched band.

Finally, a conclusion is presented and some suggestions for future work are proposed.

CHAPTER ONE

Literature Review of Radio Frequency and Microwave Theory

1.1 Introduction

The term microwave is used to describe electromagnetic (EM) waves with frequencies ranging from 300 MHz to 300 GHz, which correspond to wavelengths (in free space) from 1 m to 1 mm. The EM waves with frequencies above 30 GHz and up to 300 GHz are also called millimeter waves because their wavelengths are in the millimeter range (1–10 mm). Above the millimeter wave spectrum is the infrared. Beyond the infrared spectrum is the visible optical spectrum, the ultraviolet spectrum, and x-rays. Below the microwave frequency spectrum is the radio frequency (RF) spectrum. [4]

The majority of applications of today's microwave technology are communications systems, radar systems, environmental remote sensing, medical systems and cellular networks such as GSM, CDMA, Wi-Fi, Bluetooth, and WiMAX and satellite communication.

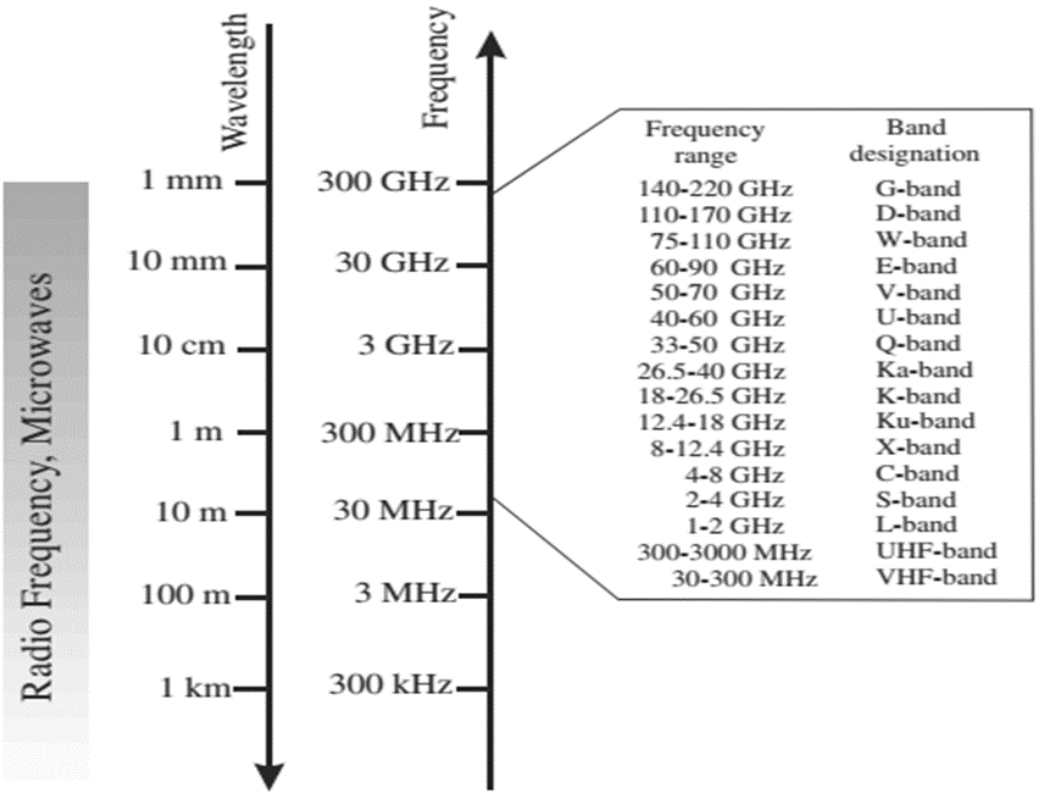

Figure I. 1: RF/Microwave spectrum [4]

1.2 Transmission Lines

Transmission line theory bridges the gap between field analysis and basic circuit theory, and so it is of significant importance in microwave network analysis. Wave propagation on transmission lines can be approached from an extension of circuit theory or from a specialization of Maxwell's equations. When both points of view are shown, it is easy to see that equations that describe wave propagation are very similar to those for plane wave propagation.

Figure I. 2 shows the different types of transmission lines [5].

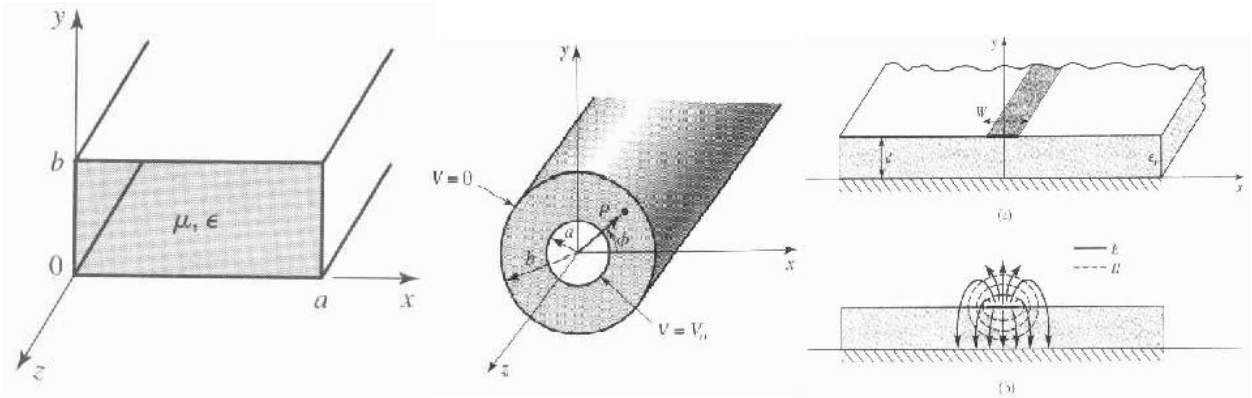

Figure I. 2: (a) waveguide, **(b)** coaxial, **(c)** Microstrip line schematics.

Table I. 1 represents a comparison between some common transmission lines [5].

Table I. 1: Comparison between common transmission lines.

Characteristic	Coaxial	Waveguide	Strip-line	Microstrip
Preferred mode	TEM	TE10	TEM	Quasi-TEM
Dispersion	None	Medium	None	Low
Bandwidth	High	Low	High	High
Loss	Medium	Low	High	High
Power capacity	Medium	High	Low	Low
Physical size	Large	Large	Medium	Small
Ease of fabrication	Medium	Medium	Easy	Easy
Ease of integration	Hard	Hard	Fair	Easy

1.3 The Microstrip line

1.3.1 Overview

Microstrip line is one of the most popular types of planar transmission lines, primarily because it can be fabricated by photolithographic processes and is easily integrated with other active and passive microwave devices. [6]

1.3.2 History

Microstrip is type of transmission line, according to Encyclopedia, it was developed by ITT Laboratories by Grieg and Engelmann in December 1952 as challenger to stripe line, due to the fields within two guided-wave media, the Microstrip does not support a pure TEM wave which makes results unpredictable, the thin version of Microstrip became popular in 1960s.

1.3.3 Structure

Microstrip transmission line consists of a conductor printed on top of thin, grounded dielectric substrate as it is illustrated in **Figure I. 3**. The property of the conductor associates with the dielectric filling dictate the signal transmission characteristics of the line. It has some (usually most) of its field lines in the dielectric region, concentrated between the strip conductor and the ground plane, and some fraction of them in the air region above the substrate. The relative permittivity of the material ε_r is almost always greater than unity resulting the fields in air propagate faster than the fields within the dielectric (different phase velocities). For this reason, the Microstrip line cannot support a pure transverse electromagnetic (TEM) wave [3].

The exact fields of a Microstrip line constitute a hybrid TM-TE wave, and require advanced analysis techniques for its characterization.

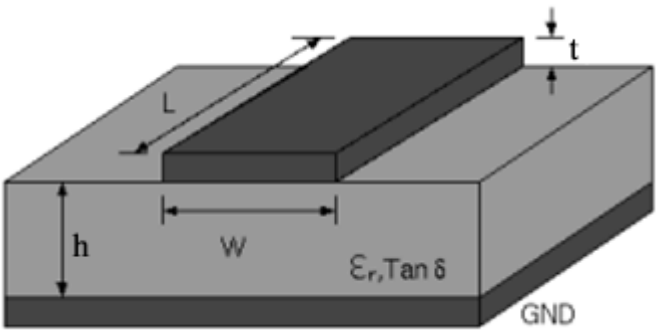

Figure I. 3: Microstrip dimensions scheme

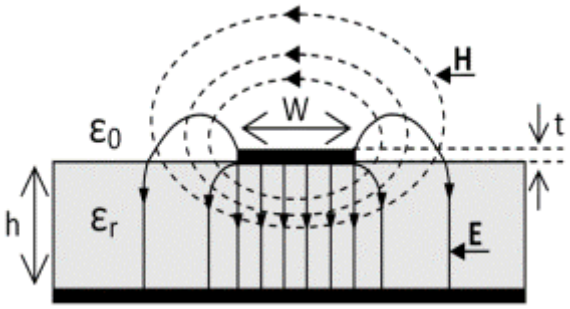

Figure I. 4: Side on view of excited Microstrip line with corresponding electric (solid lines) and magnetic (dashed lines) fields

1.3.4 Analysis Formulas

a) Effective Dielectric Constant

Dielectric constant is a measure of the extent to which it concentrates electrostatic lines of flux. Because part of the fields from the microstrip conductor exists in air, the effective dielectric constant (ε_{eff}) is somewhat less than the substrate's dielectric constant ε_r (also known as the relative permittivity).

Knowing that W is the strip width and h is the substrate thickness, the effective dielectric constant of the microstrip is calculated as follows [1]:

- When $(\frac{W}{h}) < 1$

$$\varepsilon_{eff} = \frac{\varepsilon_r + 1}{2} + \frac{\varepsilon_r - 1}{2}\left[\left(1 + 12\frac{h}{W}\right)^{-\frac{1}{2}} + 0.04\left(1 - \frac{W}{h}\right)^2\right] \qquad (I.1)$$

- When $(\frac{W}{h}) \geq 1$

$$\varepsilon_{eff} = \frac{\varepsilon_r + 1}{2} + \frac{\varepsilon_r - 1}{2}\left(1 + 12\frac{h}{W}\right)^{-\frac{1}{2}} \qquad (I.2)$$

The effective dielectric constant is seen to be a function of the ratio of the width (W) to the height (h) of a microstrip line (W/h), as well as the dielectric constant of the substrate material (ε_r) and there are separate solutions for cases where (W/h) is less than 1, and when (W/h) is greater than or equal to 1. These equations provide a reasonable approximation for ε_{eff} (effective dielectric constant). This calculation ignores strip thickness and frequency dispersion, but their effects are usually small.

b) Characteristic Impedance

The characteristic impedance of the microstrip is calculated as follows [7]:

- When $(\frac{W}{h}) < 1$

$$Z_0 = 60 * \left(\varepsilon_{eff}\right)^{-\frac{1}{2}} * \ln\left(\frac{8h}{W} + 0.25\frac{W}{h}\right)(Ohms) \quad (I.3)$$

- When $(\frac{W}{h}) \geq 1$

$$Z_0 = \frac{120\pi\left(\varepsilon_{eff}\right)^{-\frac{1}{2}}}{\frac{W}{h} + 1.393 + 0.667\ln\left(\frac{W}{h} + 1.444\right)}\ (Ohms) \quad (I.4)$$

c) Guided Wavelength

Given that λ_0 is the wavelength in free space, the guided wavelength is given by:

$$\lambda_g = \frac{\lambda_0}{\varepsilon_{eff}}\ (m) \quad (I.5)$$

d) Propagation Constant

The propagation constant is defined as follows [5]:

$$\beta = \frac{2\pi}{\lambda_g} \quad (I.6)$$

e) Phase Velocity

Phase velocity v_p is given by [5]:

$$v_p = \frac{W}{\beta} = \frac{C}{\sqrt{\varepsilon_{eff}}}\ (^m/_s) \quad (I.7)$$

Where C is the light velocity in free space (C=$3\times10^8\ m/s$)

f) Electrical Length

For a given physical length of a microstrip $\boldsymbol{l}$, the electrical length is given as [8]:

$$\theta = \beta l \quad (I.8)$$

1.4 Microstrip discontinuities

Microstrip discontinuities generally incurred in the layout of the practical filters include steps, open-ends, gaps, bends, and junctions. Discontinuities create parasitic reactances, which affect the transmission line field distributions. The altered electric field distribution can be represented by an equivalent capacitance, and the changed magnetic field distribution can be expressed in terms of an equivalent inductance. The equivalent circuit model of the discontinuity region can be modelled accurately by extrapolating the effective dimensions and taken into account in the filter design with full-wave electromagnetic (EM) simulations [3].

1.4.1 Steps in width

The junction of two lines having different widths forms this type of discontinuity. The equivalent circuit consists of a shunt capacitance C in the plane of junction and series inductors L1 and L2 on either side of it as shown in **Figure I. 5**:

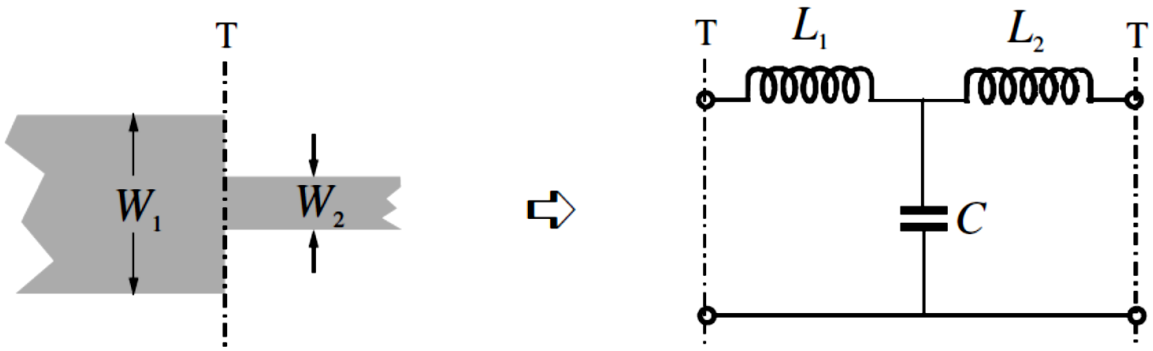

Figure I. 5: Microstrip discontinuity: Step in width and its equivalent circuit

For a symmetrical step, the capacitance and inductance may be approximated by using the following formulas [9]:

$$\frac{C}{\sqrt{W_1 W_2}}\left({}^{pF}/_{m}\right) = (4.386\ln(\varepsilon_r) + 2.33)\frac{W_2}{W_1} - 5.472\ln(\varepsilon_r) - 3.17 \qquad (I.9)$$

$$\frac{L}{H}\left({}^{nH}/_{m}\right) = 40.5\left(\frac{W_2}{W_1} - 1.0\right) - 32.57\ln\left(\frac{W_2}{W_1}\right) + 0.2\left(\frac{W_2}{W_1} - 1\right)^2 \qquad (I.10)$$

$$L_1(nH) = \frac{L_{w1}}{L_{w1}+L_{w2}}L \quad \text{and} \quad L_2(nH) = \frac{L_{w2}}{L_{w1}+L_{w2}}L \qquad (I.11\ a,b)$$

With:

$$L_{wi} = Z_{ci}\sqrt{\frac{\varepsilon_r}{C}} \qquad (I.12)$$

1.4.2 Open-ends

Open ends are encountered whenever a microstrip is open terminated. At the Open-end of a microstrip line with a width of W, the fields do not stop abruptly, instead, they extend slightly further because of the effect of fringing field.

The closed form expression for apparent increase Δl in line length due to the open-end capacitance as illustrated in **Figure I. 6** is given as follows [9]:

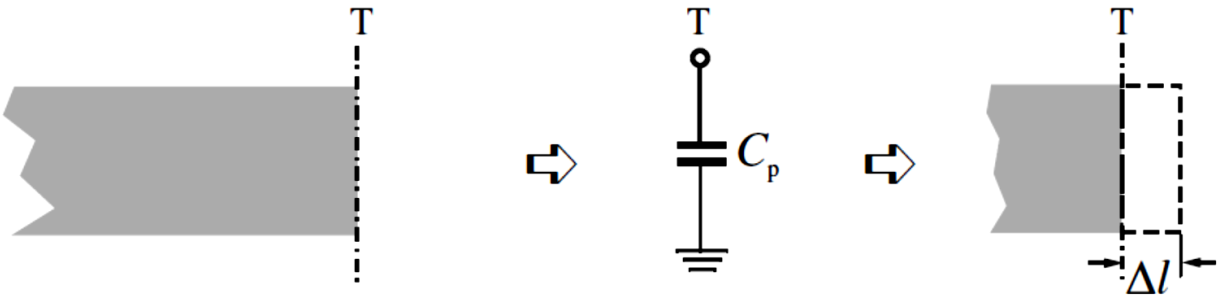

Figure I. 6: Microstrip discontinuity: Open-end and its equivalent circuit

$$\frac{\Delta l}{h} = 0.412\left(\frac{\varepsilon_{eff}+0.3}{\varepsilon_{eff}-0.258}\right)\left(\frac{\frac{W}{h}+0.264}{\frac{W}{h}+0.8}\right) \qquad (I.13)$$

Where ε_{eff} is the effective dielectric constant. For W/h ≥0.2 and $2 \leq \varepsilon_{eff} \leq 50$, yield results which are within 4 percent of the numerical results.

The open-circuit capacitance C_p may be obtained from the value of Δl/h by using the following equation:

$$\frac{C_p}{W} = \frac{\Delta l}{h}\frac{1}{W/h}\frac{\sqrt{\varepsilon_{eff}}}{cZ_0} \qquad (I.14)$$

Where c is the velocity of light in free space and ε_{eff} is the effective dielectric constant corresponding to the impedance Z_0.

1.4.3 Gaps

Corresponding susceptances as demonstrated in **Figure I. 7** can be obtained from the equivalent circuit capacitances C_g and C_p. If the two transmission lines are identical, then a plane of circuit symmetry exists and it can be analyzed using odd/even mode analysis. The incident wave along the transmission lines are opposite (equal magnitude but 180^0 out of phase) in the odd mode namely anti-symmetrical and equal (equal magnitude and equal phase) in the even mode so-called symmetrical. These are expressed in terms of C_{even} and C_{odd} as follows [9]:

$$C_p = \frac{1}{2} C_{even} \qquad (I.15)$$

$$C_g = \frac{1}{2}\left(C_{odd} - \frac{1}{2} C_{even}\right) \qquad (I.16)$$

Where C_{even} and C_{odd} are the equivalent circuit parameters for the gap when it is excited symmetrically and anti-symmetrically by creating virtually open and ground plane at the plane of circuit symmetry, respectively.

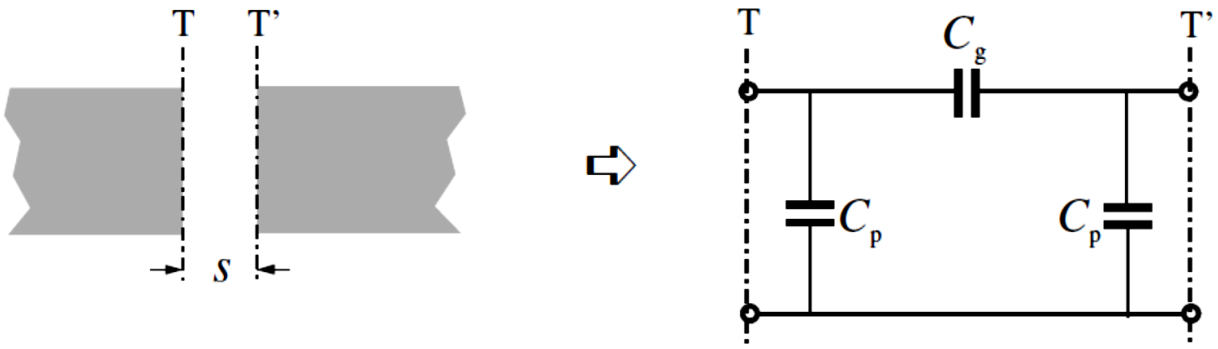

Figure I. 7: Microstrip discontinuity: Gap and its equivalent circuit

The closed form expressions for C_{even} (C_e) and C_{odd} (C_o) for ε_r=9.6 and $0.5 \leq W/h \leq 2$ are:

$$\frac{C_0}{W}(pF/m) = \frac{S}{W} m_0 \exp(K_0) \qquad (I.17)$$

$$\frac{C_e}{W}(pF/m) = \frac{S}{W} m_e \exp(K_e) \qquad (I.18)$$

Where:

$$m_0 = \frac{W}{h}\left(0.267 \ln\left(\frac{W}{h}\right) - 0.3853\right), K_0 = 4.26 - 0.631 \ln\left(\frac{W}{h}\right) for\ 0.1 \leq \frac{S}{W} \leq 1.0 \ (I.19a,b)$$

$$m_e = 0.8675, K_e = 2.043 * \left(\frac{W}{h}\right) * 0.12 \ \left(for\ 0.1 \leq \frac{S}{W} \leq 0.3\right) \qquad (I.20)$$

The values of C_e and C_o for other values of ε_r in the range $2.5 \leq \varepsilon_r \leq 15$ can be calculated by using the following scaling relations:

$$C_e(\varepsilon_r) = C_e(9.6) * \left(\frac{\varepsilon_r}{9.6}\right) * 0.9 \qquad (I.21)$$

$$C_0(\varepsilon_r) = C_0(9.6) * \left(\frac{\varepsilon_r}{9.6}\right) * 0.8 \qquad (I.22)$$

1.4.4 Bends

Bends are the most frequently encountered discontinuities in a microstrip. The simplest bends are the ones with angles equal to or greater than 90°, which do not work well above few GHz, due to a high VSWR. The effect of a bend discontinuity increases with the frequency, the number of bends used in cascade, and the line width.

Microstrip right-angle band may be designed by an equivalent T-network as illustrated in **Figure I. 8**.

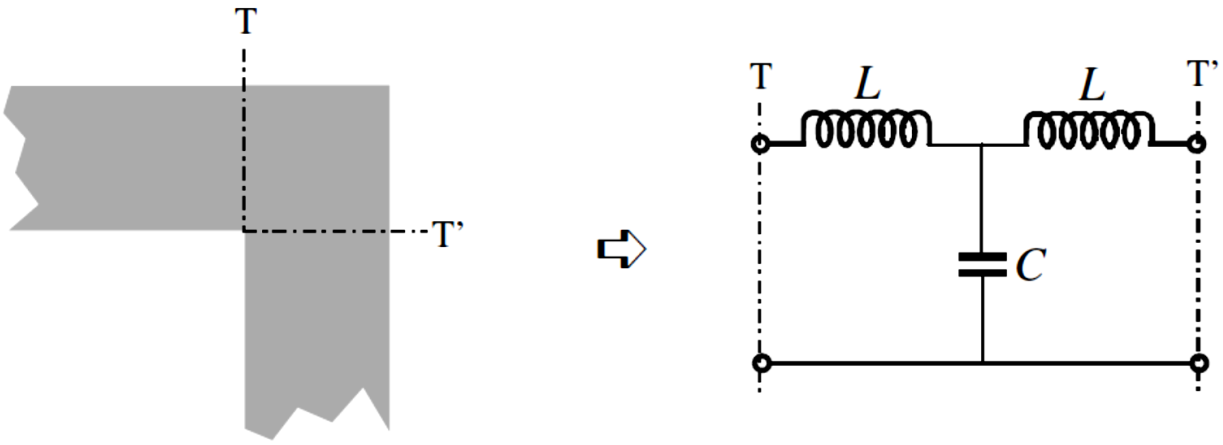

Figure I. 8: Microstrip discontinuity: Bend and its equivalent circuit

The closed form equations are given as follows [4]:

$$\frac{C}{W_1}\left(^{pF}/_{m}\right) = \left[\frac{(4\varepsilon_r + 12.5)\,W/h - (1.83\varepsilon_r - 2.25)}{\sqrt{W/h}} + \frac{0.02\varepsilon_r}{W/h}\right] \quad for\ W/h \leq 1$$

$$= (9.25\varepsilon_r + 1.25)\,W/h + 5.2\varepsilon_r + 7.0 \qquad for\ W/h \geq 1 \qquad (I.23)$$

$$\frac{L}{h}\left(^{nH}/_{m}\right) = \left[100\left(4\sqrt{\frac{W}{h} - 4.21}\right)\right] \qquad (I.24)$$

1.5 Microstrip Coupled Lines

Coupled microstrip lines are widely used for implementing microstrip filters. **Figure I. 9** illustrates the cross section of a pair of coupled microstrip lines, where the two microstrip lines of width 'W' are in the 'parallel' or 'edge coupled' configuration with a separation S [10].

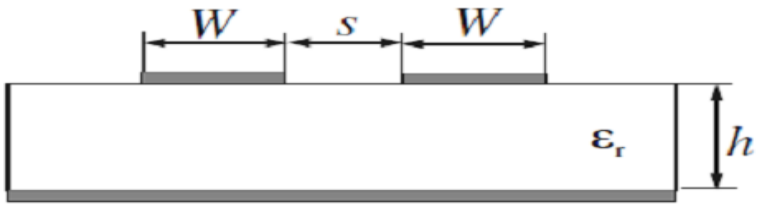

Figure I. 9: Cross section view of coupled microstrip lines

These lines are the basic building elements of directional couplers and filters. There is continuous coupling between electromagnetic fields of the lines. The field distribution of the coupled microstrip lines is shown in **Figure I. 10**.

For these coupled lines, there are two special types of excitations:

- **Even mode**, where the currents in the strip conductors are equal in amplitude and in the same direction.
- **Odd mode**, where the currents in the strip conductors are equal in amplitude and in opposite directions.

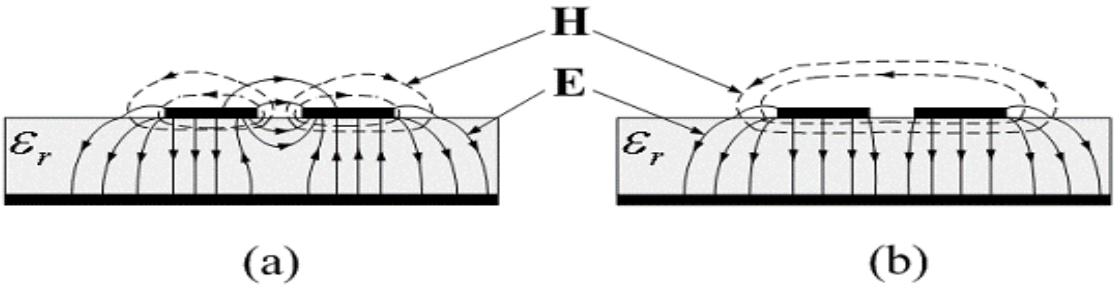

Figure I. 10: Field distribution of coupled microstrip lines: (a) Odd mode; (b) Even mode

In a static approach similar to the single microstrip, the even- and odd-mode characteristic impedances and effective dielectric constants of the coupled microstrip lines may be obtained in terms of the even- and odd-mode capacitances, denoted by C_e and C_o. As shown in **Figure I. 11**.

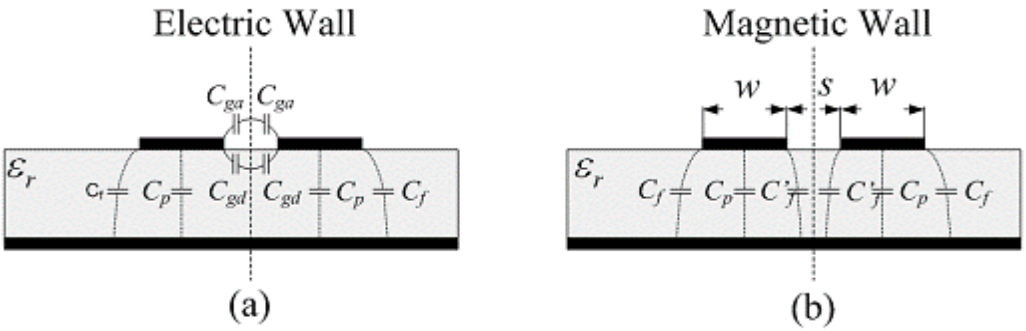

Figure I. 11: Distributed capacitances: **(a)** Odd mode; **(b)** Even mode

The Even and Odd mode capacitances C_e and C_o are expressed as follows [11]:

$$C_e = C_p + C_f + C'_f \qquad (I.25)$$

$$C_0 = C_p + C_f + C_{gd} + C_{ga} \qquad (I.26)$$

In these expressions, C_p denotes the parallel plate capacitance between the strip and the ground plane. It is defined as:

$$C_p = \varepsilon_0 \varepsilon_r \frac{W}{h} \qquad (I.27)$$

C_f is the fringe capacitance as if for an uncoupled single microstrip line, the term C_f accounts for the modification of fringe capacitance C_f of a single line due to the presence of another line. For the odd-mode, C_{ga} and C_{gd} represent, respectively, the fringe capacitances for the air and dielectric regions across the coupling gap. The capacitance C_{gd} may be found from the corresponding coupled strip line geometry, with the spacing between the ground planes given by 2h. C_{ga} can be modified from the capacitance of the corresponding coplanar strips.

1.6 Defected Ground Structure (DGS)

1.6.1 Definition

In recent years, there have been several new concepts applied to distributed microwave circuits; one of them is the defected ground structure. DGS is a deliberately etched periodic or non-periodic cascaded configuration in ground plane metal of a microstrip (or Strip-line, or coplanar waveguide) or transmission line [12], it disturbs the shield current distribution in the ground plane which eventually changes the characteristics of a transmission line such as line capacitance and line inductance. Also, it increases the characteristic impedance of microstrip so; wider microstrip line may be used, this may lead to higher power capabilities from the transmitter. It also provides band rejection in certain frequency bands, which can be called as band-gap or stop

band effect. The DGS has been applied to design microwave circuits such as microwave filters, power divider, couplers, amplifiers, oscillators and so on by using different patterns of DGS underneath the microstrip line, so the DGS is used to achieve the reduction in size and improve the performance of microstrip components [13].

1.6.2 DGS Models

Many various DGS shapes have been studied such as dumbbells, U and V shaped slots, spiral and concentric ring circles. Each DGS form can be represented as a circuit consisting of inductance and capacitance, which may lead to a certain frequency band gap determined by the shape, dimensions and even the position of the defect.

Figure I. 12 and **Figure I. 13** illustrate different DGS types [14].

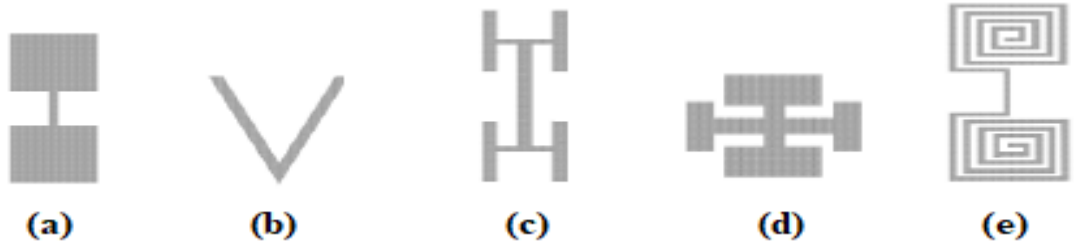

Figure I. 12: DGS models: **a)** dumbbell-shaped, **b)** V-shaped, **c)** H-shaped, **d)** Cross-shaped **e)**Spiral shaped

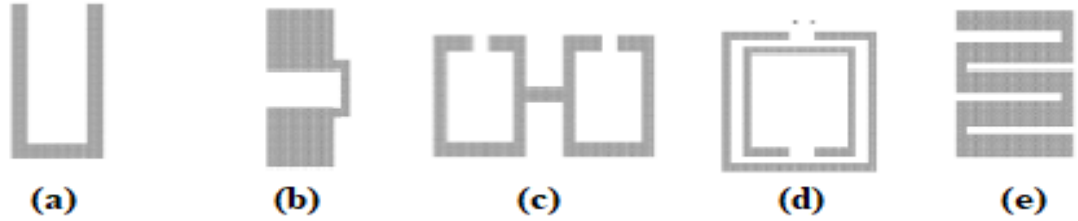

Figure I. 13: DGS models **a)** U-shaped, **b)** square heads connected with U slots, **c)** open loop dumbbell, **d)** split ring resonator, **e)** meander line

1.6.3 Equivalent Circuit

DGS may be considered as an equivalent circuit consisting of resistance (R), inductance (L) and capacitance (C). The equivalent circuit for a DGS is a parallel tuned circuit in series with the transmission line to which it is coupled.

Figure I. 14 shows the circuit model of the DGS [15], the input and output impedances are that of the transmission line and the equivalent values of R, L and C are determined by the dimensions of the DGS structure and its position relative to the transmission line. The circuit parameters of the equivalent circuit are calculated using the following expressions [16]:

$$C = \frac{\omega_c}{2Z_{0(\omega_0^2 - \omega_c^2)}} \quad (I.28)$$

$$L = \frac{1}{{\omega_0}^2 C} \quad (I.29)$$

$$R = \frac{2Z_0}{\sqrt{\frac{1}{|s_{11}(\omega_0)|^2} - \left(2Z_0\left(\omega_0 C - \frac{1}{\omega_0 L}\right)\right)^2 - 1}} \quad (I.30)$$

Where $(\omega_0 = 2\pi f_0)$ and $(\omega_c = 2\pi f_c)$ are respectively the angular resonant and -3 dB cut-off frequencies of the DGS pattern. Z_0 is the characteristic impedance of the microstrip transmission line.

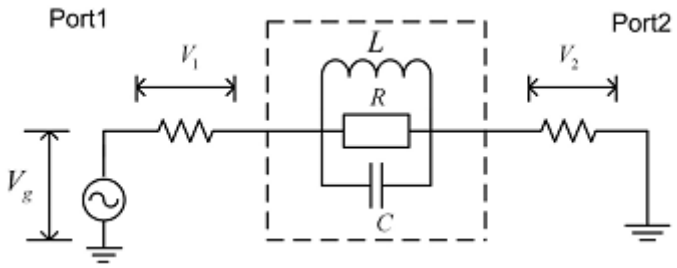

Figure I. 14: RLC equivalent circuit for DGS

1.7 Scattering Parameters

Scattering parameters or S-parameters (the elements of a scattering matrix or S-matrix) describe the electrical behavior of linear electrical networks when undergoing various steady state stimuli by electrical signals. The parameters are useful for several branches of electrical engineering, including electronics, communication systems, and especially for microwave engineering [17].

In the context of S-parameters, scattering refers to the way in which the traveling currents and voltages in a transmission line are affected when they meet a discontinuity caused by the insertion of a network into the transmission line. This is equivalent to the wave meeting an impedance differing from the line's characteristic impedance.

Although applicable at any frequency, S-parameters are mostly used for networks operating at radio frequency (RF) and microwave frequencies where signal power and energy considerations are more easily quantified than currents and voltages.

S-parameters are readily represented in matrix form and obey the rules of matrix algebra.

Figure I. 15 represents two ports S-parameter network.

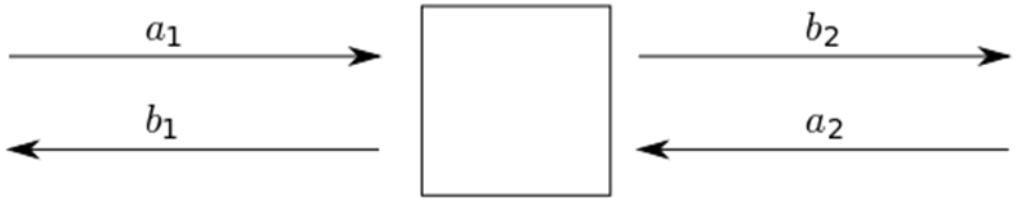

Figure I. 15: S-parameters two ports network

In this case the relationship between the reflected, incident power waves and the S-parameter matrix is given by:

$$\begin{pmatrix} b_1 \\ b_2 \end{pmatrix} = \begin{pmatrix} S_{11} & S_{12} \\ S_{21} & S_{22} \end{pmatrix} \begin{pmatrix} a_1 \\ a_2 \end{pmatrix}$$

Expanding the matrices into equations gives:

$$b_1 = S_{11}a_1 + S_{12}a_2 \qquad (I.31a)$$

$$b_2 = S_{21}a_1 + S_{22}a_2 \qquad (I.31b)$$

The 2-port S-parameters have the following generic descriptions:

- S_{11} is the input port reflection coefficient.
- S_{12} is the reverse transmission (insertion) gain.
- S_{21} is the forward transmission (insertion) gain.
- S_{22} is the output port reflection coefficient.

1.8 Advantages and disadvantages of Microstrip technology

Microstrip line are widely used in the manufacturing of microwave components due to some suitable features. This technology has advantages such as simple geometry, less expensive, lighter, supports very high frequencies, presents high selectivity, more compact and easier than other technologies to integrate in active devices.

In the other hand it possesses some disadvantages such as high losses, low power handling capacity, unintentional radiation and cannot be used when the distance between source and load is long.

CHAPTER TWO

Theory of Filters

And

UWB Technology

2.1 Introduction

A microwave filter is a two-port network used to control the frequency response at a certain point in a microwave system. It provides transmission at frequencies within the pass-band of the filter and attenuation in the rest of the band, the stop-band. Typical frequency responses include low-pass, high-pass, bandpass and band-reject characteristics.

Microstrip Filters for RF/Microwave Applications offers a unique and comprehensive treatment of RF/microwave filters based on the microstrip structure, providing a link to applications of computer-aided design tools and advanced materials and technologies. Many novel and sophisticated filters are designed using computer-aided design, from basic concepts to practical realizations [4].

2.2 Filter Parameters

In analyzing the various trade-offs when dealing with filters, the following parameters play key roles, giving information of its main characteristics:

2.2.1 Transfer Function

Transfer functions are commonly used in the analysis of systems such as single-input and output filters, typically within the fields of signal processing, communication theory, and control theory.

The transfer function of a two-port filter network describes mathematically the characteristics of the network response as an expression of S_{21}. Usually, an amplitude-squared transfer function for a lossless passive filter network is defined as [18]:

$$|S_{21}(j\omega)|^2 = \frac{1}{1 + \varepsilon^2 F_n^2(\omega)} \qquad (II.1)$$

Where ε is the ripple constant, $F_n(\omega)$ represents a characteristic or filtering function, and ω is a frequency variable.

2.2.2 Insertion Loss

Ideally, a perfect filter would introduce no power loss in the passband. It would have zero insertion loss. But in reality, we have to expect a certain amount of power loss associated with the filter. The insertion loss quantifies how much below the 0 dB line the power amplitude response drops.

Insertion Loss (IL), in dB, is expressed as:

$$IL(dB) = -10log_{10}\left(\frac{P_{out}}{P_{in}}\right) \qquad (II.2a)$$

Where P_{out} and P_{in} are, respectively, the output and input powers.

Using S-Parameters, it is expressed as follows [5]:

$$IL(dB) = -20log_{10}|S_{21}| \qquad (II.2b)$$

2.2.3 Return Loss

Return loss (RL) is the loss of power in the signal reflected by a discontinuity in a transmission line. This discontinuity can be a mismatch with the terminating load or with a device inserted in the line. It is usually expressed as a ratio in decibels (dB):

$$RL(dB) = -10log_{10}\left(\frac{P_{in}}{P_R}\right) \qquad (II.3a)$$

Where P_{in} is input power and P_R is reflected power.

Using S-Parameters, it is expressed as follows [19]:

$$RL(dB) = -20log_{10}|S_{11}| \qquad (II.3b)$$

2.2.4 Bandwidth

Bandwidth in hertz is an important concept in different fields: electronics, digital communications, information theory, signal processing, radio communications, and spectroscopy. It determines the capacity of a given communication channel. The bandwidth is the difference between the upper and lower frequencies in a continuous set of frequencies relative to 3 dB attenuation point.

It is expressed as follows:

$$BW(Hz) = f_{-3dB(upper)} - f_{-3dB(lower)} \qquad (II.4)$$

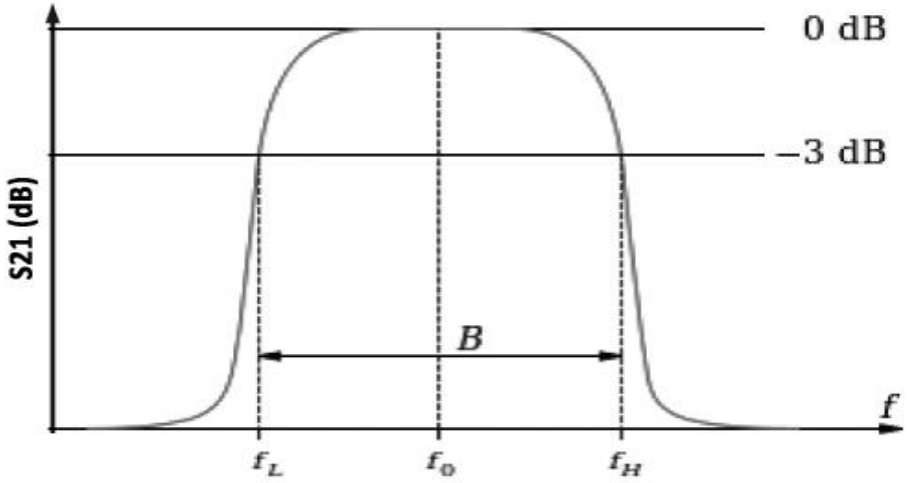

Figure II. 1: 3 dB Bandwidth illustrated between the upper and the lower frequencies f_H and f_L

2.2.5 Center Frequency

The center frequency of a filter or channel is a measure of a central frequency between the upper and lower cutoff frequencies. it is defined as either the arithmetic or the geometric mean of the lower and the upper cutoff frequencies.

The geometric mean value is calculated as follows:

$$f_0(Geometric) = \sqrt{f_{-3dB_{upper}} * f_{-3dB_{lower}}} \qquad (II.5a)$$

The arithmetic mean value is calculated as follows:

$$f_0(Arithmetic) = \frac{f_{-3dB_{upper}} + f_{-3dB_{lower}}}{2} \qquad (II.5b)$$

2.2.6 Cutoff Frequency

The cutoff frequency (f_c) is defined as the frequency at which the ratio of the (input/output) power has a magnitude of one half (0.50). In decibel (–3 dB), or at which the insertion loss of a filter is equal to 3dB.

2.2.7 Fractional Bandwidth

The fractional bandwidth (FBW) is a factor used to classify signals as narrowband, wideband, or ultra-wide band. It is defined as being the ratio of bandwidth at -10 dB level to the center frequency.

It is calculated using the following formula:

$$FBW(\%) = \frac{BW}{f_0} * 100\% \qquad (II.6)$$

Where

$$BW = f_h - f_l \quad and \quad f_0 = \frac{f_h + f_l}{2}$$

With f_h and f_l being the highest and the lowest cutoff frequencies at (-10 dB level).

The classification of signals based on their fractional bandwidth is stated as follows [20]:

$\boldsymbol{FBW < 1\%}$	**Narrow band**
$\boldsymbol{1\% < FBW < 20\%}$	**Wide band**
$\boldsymbol{FBW > 20\%}$	**Ultra-wide band**

Figure II. 2 illustrates the fractional spectrum bandwidth for Ultra-wideband case.

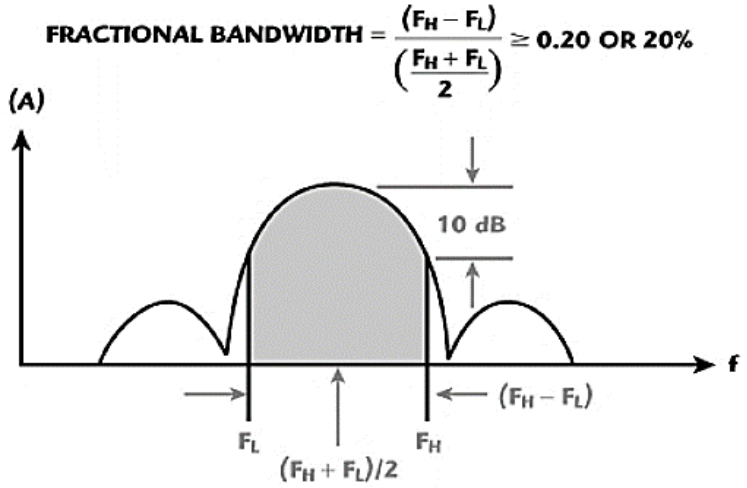

Figure II. 2: Fractional spectrum bandwidth

2.2.8 Quality Factor

The unloaded quality factor (Q) is defined as being the center frequency-to-bandwidth ratio expressed as:

$$Q = \frac{f_0}{BW} \qquad (II.7)$$

It is noticed that the higher the Q is, the narrower and 'sharper' the peak is. It is the inverse of the fractional bandwidth.

2.3 Types of Filters

In circuit theory, a filter is an electrical network that alters the amplitude and/or phase characteristics of a signal with respect to frequency. Ideally, a filter will neither add new frequencies to the input signal, nor change it. However, it will vary the relative amplitudes of the various frequency components and/or their phase relationships. Filters are used to allow some frequencies to pass through a desired band while they attenuate the others. According to their applications, we distinguish the following classes [21]:

2.3.1 Low pass Filter

A low-pass filter (LPF) is a filter that passes signals with a frequency lower than a certain cutoff frequency and attenuates (reduces the amplitude of) signals with frequencies higher than the cut-off frequency (fc). the output at the critical frequency is 70.7% of the input. This response is equivalent to an attenuation of -3dB. The actual amount of attenuation varies from filter to other. **Figure II. 3** illustrates a practical response of an LPF.

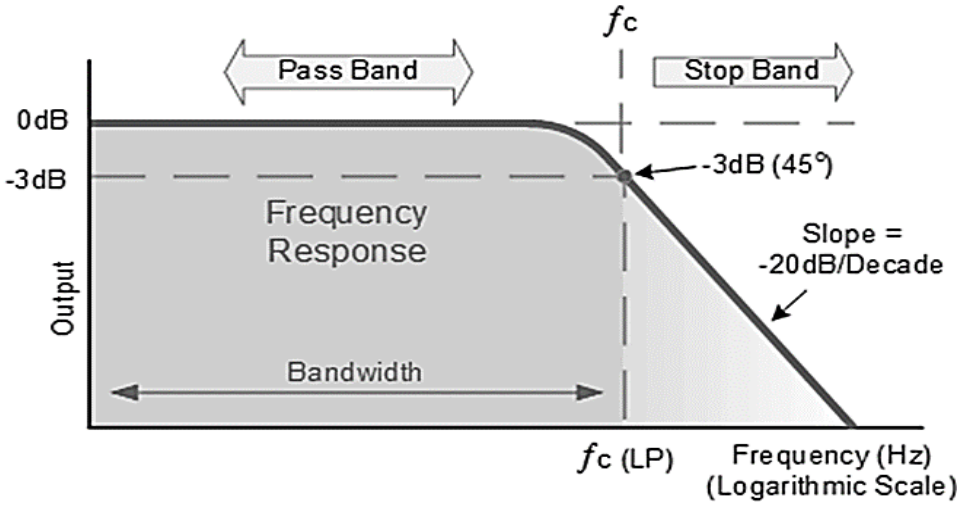

Figure II. 3: Practical response of an LPF

2.3.2 High pass filter

A high-pass filter (HPF) passes high frequencies and attenuates (reduces the amplitude) frequencies lower than the cutoff frequency, so no more than the opposite of an LPF. The actual amount of attenuation for each frequency depends on the design parameter of the filter. HPFs are used in digital image processing to perform image modifications, enhancements, noise reduction, and the conjunction of it with an LPF produces a band-pass filter.

Figure II. 4 illustrates a practical response of an HPF.

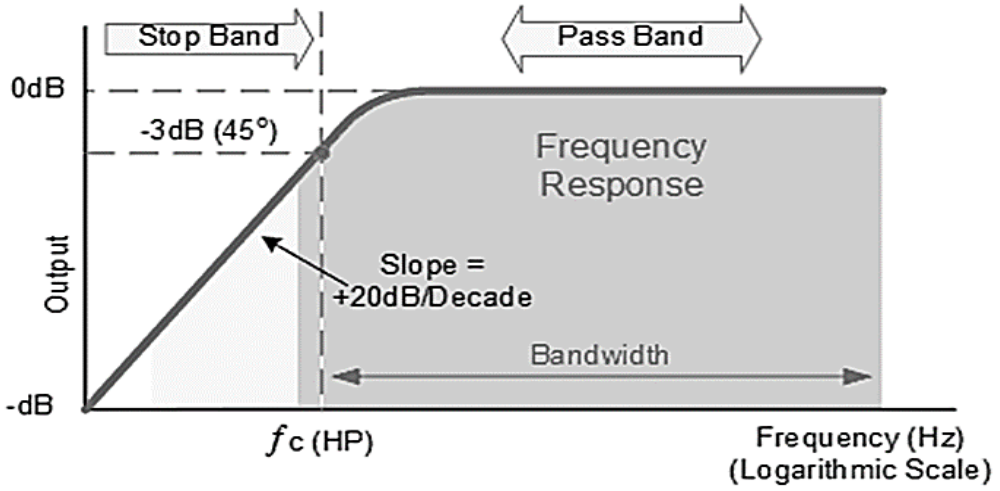

Figure II. 4: Practical response of an HPF

2.3.3 Bandpass Filter

A band-pass filter (BPF) passes frequencies within certain range and rejects (attenuates) frequencies outside that range.

An ideal BPF would have a completely flat pass-band (e.g. with no gain/attenuation throughout) and would completely attenuate all frequencies outside the pass-band. Additionally, the transition out of the pass-band would be instantaneous in frequency. In practice, no band-pass filter is ideal. The filter does not attenuate all frequencies outside the desired frequency range completely; in particular, there is a region just outside the intended pass-band where frequencies are attenuated, but not rejected.

Figure II. 5 illustrates a practical response of a BPF.

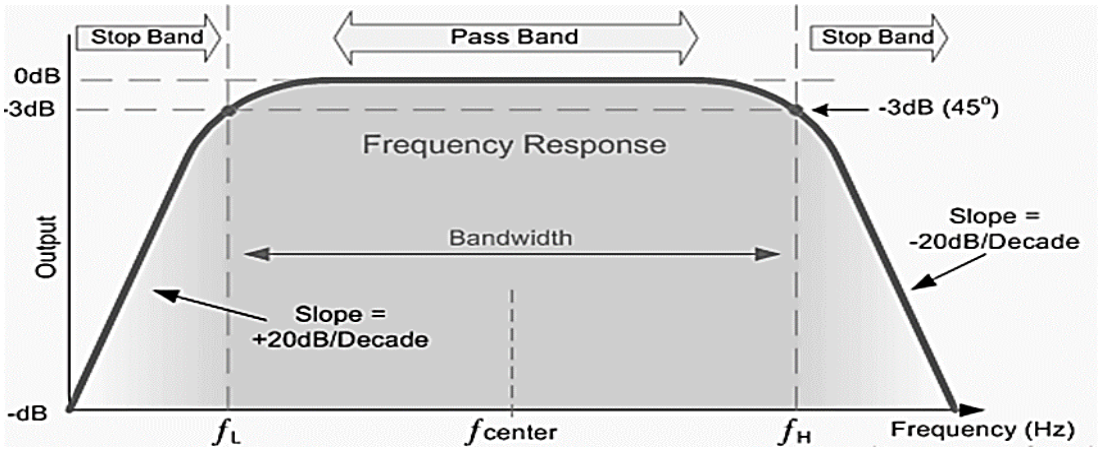

Figure II. 5: Practical response of a BPF

2.3.4 Band-reject or Band-stop Filter

A band-stop filter or band-reject filter is a filter that passes most frequencies unaltered, but attenuates those in a specific range to very low levels. It is the opposite of a bandpass filter.

Figure II. 6 illustrates a practical response of a Band-reject Filter (BRF).

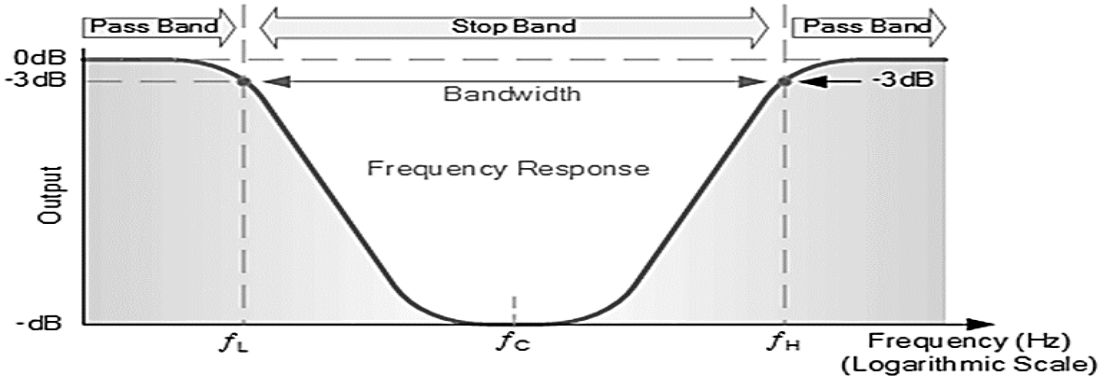

Figure II. 6: Practical response of a BRF

2.4 Ultra-Wide Band (UWB) Technology

2.4.1 Historical perspective

UWB communications is not a new technology. It was first employed by G. Marconi in 1901 to transmit Morse code sequences across the Atlantic Ocean using spark gap radio transmitters. However, the benefit of a large bandwidth and the capability of implementing multi-user systems provided by electromagnetic pulses were never considered at that time.

Approximately 50 years after G. Marconi, modern pulse-based transmission gained momentum in military applications in the form of impulse radars. The genesis of UWB technology is a result of the research works in time-domain electromagnetics that began in 1962. The concept was to characterize linear, time-invariant (LTI) systems by their output response to an impulse excitation, instead of the more conventional means of swept frequency response (i.e., amplitude and phase measurements versus frequency). It was not possible to measure the impulse response directly until the development of impulse excitation and measurement techniques. Once these techniques were in place, it became obvious that these could be used for short pulse radar and communication systems.

Many of the communication technologies were first experimented and used in military applications for some decades, only to be used for commercial applications at a much later time. UWB is no exception to this trend. From the 1960s to the 1990s, this technology was restricted to military and Department of Defense (DoD) applications under classified programs such as highly secure communications. In 1978, G.F. Ross and C.L. Bennett applied these techniques for radar and communication applications. This technology was referred to as base-band, carrier-free, or impulse until the late 1980s and was termed UWB by the U.S. DoD around 1989. By that time, UWB theory had experienced 30 years of development [22].

Although UWB technology is old, its application for communication is relatively new. The recent advancements in microprocessor and fast switching in semiconductor technology has made UWB ready for commercial applications. Therefore, it is more appropriate to consider UWB as a new name for a long-existing technology. As interest in the commercialization of UWB has increased over the past several years, developers of UWB systems began pressuring the FCC to approve UWB for commercial use.

2.4.2 Definition

Ultra-wideband (UWB) wireless communication is a revolutionary technology for transmitting large amounts of digital data over a wide frequency spectrum using short-pulse, low powered radio signals. UWB commonly refers to a signal or system that either has a large relative

bandwidth (BW) that exceeds 20% or a large absolute bandwidth of more than 500 MHz [20]. A "14 February 2002" Report and Order by the Federal Communications Commission (FCC) authorizes the unlicensed use of UWB in 3.1–10.6 GHz. This is intended to provide an efficient use of scarce radio bandwidth while enabling both high data rate personal area network (PAN) wireless connectivity and longer-range, low data rate applications as well as radar and imaging systems.

To allow coexistence, power regulations for this technology were also strictly defined. The maximum of emitted power must be under -41.3 dBm/MHz. This is equivalent to 75 nW/MHz of average continuous power transmission.

Figure II. 7 illustrates the spectral distribution of UWB system and other systems.

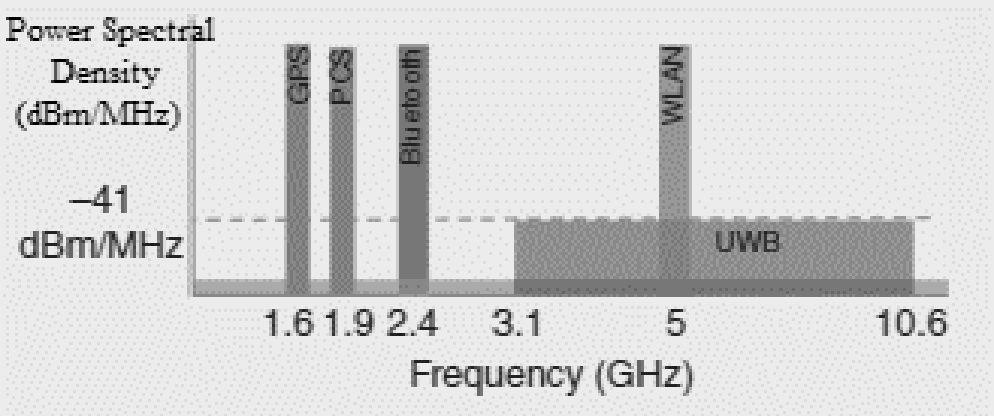

Figure II. 7: Spectral distribution of UWB system and other narrowband systems

2.4.3 Advantages

Future generations of communication systems will require high mobility, flexibility, and very high data-rate. In this context, broadband wireless digital communication is inevitable. As the capacity of the channel is directly related to its bandwidth, UWB technologies are advantageous for use in a number of wireless communication applications. Some of the advantages are [22]:

- Coexistence with current narrowband and wideband radio services and thus, avoiding expensive licensing fees.
- Low power transmission which provides high degree of security with low probability of detection and inspection.
- High performance in multipath channels which leads to delivering higher signal strengths in adverse conditions.

- Large channel capacity, thus, high bandwidth can support real time high definition video streaming
- Ability to work with low signal to noise ratio (SNR). As a result, offering high performance in noisy environments.
- Simple transceiver architecture which enables ultra-low power, smaller form factor, and better mean time between failures, all at reduced cost.
- Resistance to jamming which leads to reliability in hostile environments.

2.4.4 Disadvantages

Some of the disadvantages of this promising technology includes [22]:

- **Interference:** Interference is one of the major challenges in the design of UWB communication systems. Since UWB communication devices occupy a large frequency spectrum, interference avoidance with coexisting users is one of the key issues of UWB technology. Existing electronic devices include current IEEE 802.11a WLAN devices (working at 5.150–5.825 GHz) and 2.4 GHz industrial, scientific, and medical (ISM) band devices, that are used by wireless personal area networks like Bluetooth.
- **Complex signal processing:** For narrowband systems that use carrier frequency, frequency-division multiplexing is very straightforward and the development of a narrowband device needs to consider the frequency bands directly affecting it and minimizing interference to out-of-band systems by emission control techniques like filtering and wave shaping. For carrier-less transmission and reception, every narrowband signal in the vicinity is a potential interferer and also every other carrier-less system. So, any carrier-less system has to rely on relatively complex and sophisticated signal processing techniques to recover data from the noisy environment.
- **Bit Synchronization time:** since pulses with picoseconds precision are used in UWB, the time for a transmitter and receiver to achieve bit synchronization can be as high as a few milliseconds. So, the channel acquisition time is very high, which can significantly affect performance, especially for intermittent communications.
- **Short range area:** information can travel only for short distances (10-20m) due to low power transmission.

2.4.5 Applications

There are variety of applications for UWB technology. Some, like UWB radars, have been in use for many years while others are new potential applications, UWB sensor networks, and UWB positioning systems. Some of these applications involve:

a) In Radars

- Vehicular radars used for collision detection/avoidance and sensing road conditions.
- Ground penetrating radars.
- Tags identification.
- Through wall imaging used for rescue, security and medical applications.

b) In Wireless Communication Systems

- Transferring large amounts of data using wireless networks in short-range for home or office networking.
- Short range voice, data, and video applications (a television set and computer system without wires and transferring data at a higher rate than wired connections).
- Military communications, on board helicopters and aircrafts that would otherwise have too many interfering multipath components.
- Roadside information that can be deployed where the messages may contain weather reports, road conditions, construction information and emergency assistance communication.

c) In Localization and Tracking

- Accurately locating a person or object within one inch of its location through any structure; Global positioning system (GPS) technology is only accurate up to 1 m and does not work inside buildings; GPS is expensive but UWB will be low cost.
- Detecting land mines.
- Assessing enemy locations and tracking troops.
- Localization in search and rescue efforts, tracking of livestock and pets.

CHAPTER THREE

DESIGN AND IMPLEMENTATION OF UWB BAND PASS FILTER WITH AND WITHOUT DUAL NOTCHED BAND

3.1 Introduction

Following the adoption by the Federal Communications Committee (FCC) in February 2002 of the unlicensed use of ultra-wideband (UWB) communications spectrum from 3.1 GHz to 10.6 GHz, there has been increasingly interesting research on UWB techniques by academics and private industry. UWB Filters have several advantages: They have a bandwidth of 7.5 GHz, which can support a high transmission data rate; they have low energy density over a wideband spectrum generated by short pulse excitation, which not only makes the UWB system difficult to intercept but also minimizes interference by other radio systems; and they have extremely low transmission energy [23].

A UWB BPF, as one of the essential components of the UWB systems, has gained much attention in recent years. There are many techniques presented to design UWB bandpass filters. For example, multiple-mode resonator (MMR) [24], multilayer coupled structure [25], defected ground structure (DGS) [26], defected microstrip structure (DMS) [27], and the cascaded low-pass/high-pass filters [28] have been widely used to achieve UWB characteristics.

However, the existing wireless networks such as 5.8 GHz WLAN signals, and some 8.0 GHz satellite communication systems signals can easily interfere with UWB users. Therefore, compact UWB BPF with multiple notched bands is emergently required to reject these interfering signals. Some of the techniques used to generate notches employ: DGS units, embedded open-circuited stubs, asymmetric parallel coupled lines, short-circuited L-shaped stubs, and parasitic coupled lines [3].

Several works related to the design of UWB BPFs with single or multi-notches have been reported in the last decade. In [29], a notch has been created using SIR near the stepped-impedance stub-loaded resonator at 5.2 GHz to eliminate WLAN interference. Dual notched band was achieved in [30] by employing embedded open circuited stubs in the form of defected microstrip structure (DMS), another structure using E-shaped resonator has been introduced in [31].

The purpose of this work is to design, implement and measure a microstrip UWB BPF with dual notched band. The numerical, electrical and electromagnetic simulations are carried out in MATLAB, ADS, and CST. The proposed filter is fabricated on FR4 substrate ($\varepsilon_r = 4.3$, $h = 1.62$ mm, $\tan\theta = 0.017$).

3.2 Design, Analysis and Simulation of the proposed UWB bandpass filter

To design such a filter, different steps have been followed.

First, starting from a basic 50 Ω transmission line as illustrated in **Figure III. 1**, and using the Electrical simulator of ADS environment, the response shown in **Figure III. 2** has been obtained.

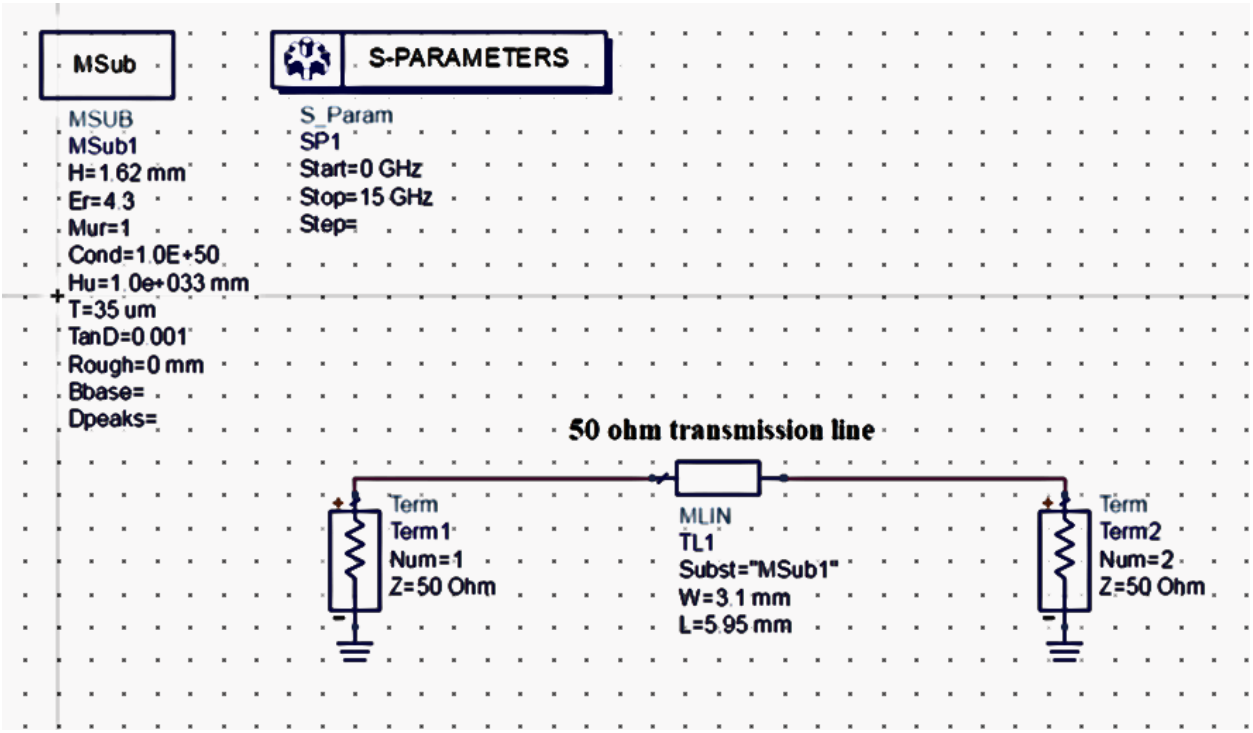

Figure III. 1: ADS Circuit Design of 50 Ohm transmission line connected to 50 Ohm ports

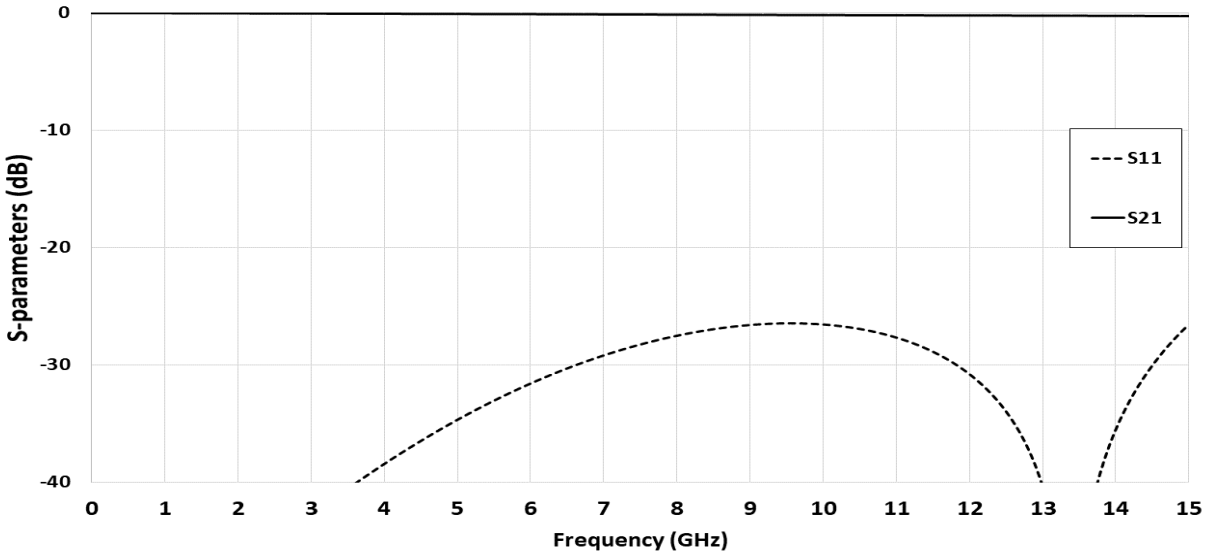

Figure III. 2: S_{11} and S_{21} responses of the 50 Ohm transmission line

As expected, since the 50 Ohm transmission line is matched to the connected 50 Ohm ports, all the signals in the given range pass from the input port to the output port, which is demonstrated by the obtained results. (The transmission coefficient **S_{21} = 0 dB** and the reflection coefficient **S_{11} << -15 dB**).

To fulfil UWB standard requirements, and to satisfy the selectivity that requires a sharp response at two cutoff frequencies of the filter pass-band, it is necessary to design a stepped impedance stub (SIS) [10] for $|S_{21}|=0$ at the frequencies $fz_1 = 3.1$ *GHz* and $fz_2 = 10.6$ *GHz.*
The stepped impedance stub is illustrated in **Figure III. 3**.

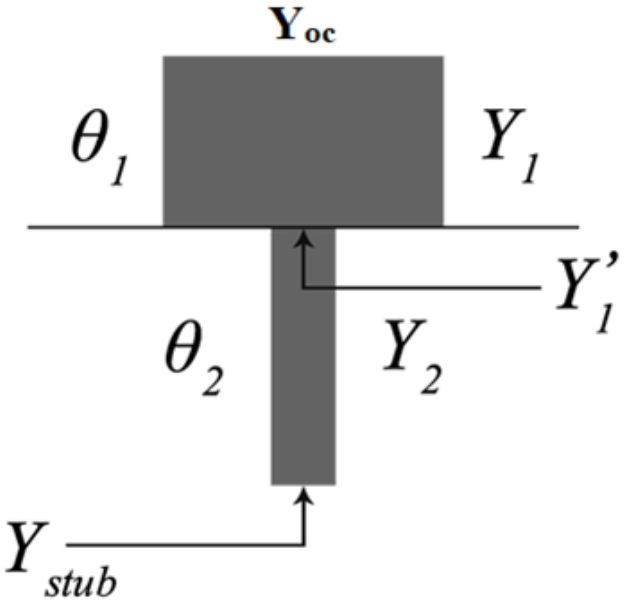

Figure III. 3: Stepped impedance Stub

fz_1 and fz_2 are the transmission zeros where $Y_{Stub}(f_{z1}) = Y_{Stub}(f_{z2}) \rightarrow \infty$ which means that at the selected frequencies the signal is shorted out through the stub.
The SIS analysis is done as follows:
Based on RF theory [6]; the input admittance Y_1' could be written as:

$$Y_1' = Y_1 \frac{Y_{oc} + jY_1 tan\theta_1}{Y_1 + jY_{oc} tan\theta_1} \qquad (III.1)$$

Where: Y_{oc} is the open circuit admittance,

Y_1 is the characteristic admittance,

θ_1 is the electrical length.

Having $Y_{oc} = 0$, leads to:

$$Y_1' = jY_1 tan\theta_1 \qquad (III.2)$$

Then, the total input admittance Y_{stub} maybe written as:

$$Y_{stub} = Y_2 \frac{Y_1' + jY_2 tan\theta_2}{Y_2 + jY_1' tan\theta_2} \qquad (III.3)$$

Where:

Y_2 is the characteristic admittance,

θ_2 is the electrical length.

Replacing Y_1' by its corresponding value gives the following:

$$Y_{stub} = jY_2 \frac{Y_1 tan\theta_1 + Y_2 tan\theta_2}{Y_2 - Y_1 tan\theta_1 tan\theta_2} \qquad (III.4)$$

It has been stated that to create a transmission zero, the total input admittance should tend to infinity ($Y_{stub} \to \infty$), which means:

$$Y_2 - Y_1 tan\theta_1 tan\theta_2 = 0 \qquad (III.5)$$

This gives the following ratio:

$$\frac{Y_2}{Y_1} = tan\theta_1 tan\theta_2 \qquad (III.6)$$

Let:

$$k = \frac{Y_1}{Y_2} = \frac{Z_2}{Z_1} \qquad (III.7)$$

An appropriate range, taking into account limitations of Microstrip technology, for characteristic impedance could be set as [32]: **20 Ohms < Z < 160 Ohms**

This leads to the following range of k: **0.125 < k < 8**

Then, **Equation III.6** could be written as:

$$k * tan\theta_1 * tan\theta_2 = 1 \qquad (III.8)$$

Where:

$$\theta_1 = \frac{2\pi}{\lambda} l_1 = \frac{2\pi}{\lambda_0}\frac{\lambda_0}{\lambda} l_1 = \theta_{01}\frac{f_{zi}}{f_0}; i = 1,2 \qquad (III.8a,b)$$

$$\theta_{01} = \beta_0 l_1 \quad ; \quad \beta_0 = \frac{2\pi}{\lambda_0} \quad ; \quad \frac{\lambda_0}{\lambda} = \frac{C/f_0}{C/f_{zi}} = \frac{f_{zi}}{f_0} \; ; i = 1,2$$

The same procedure is done for θ_2:

$$\theta_2 = \theta_{02}\frac{f_{zi}}{f_0} \; ; i = 1,2 \qquad (III.9a,b)$$

Where:

$$\theta_{02} = \beta_0 l_2 \quad ; \quad \beta_0 = \frac{2\pi}{\lambda_0} \quad ; \quad \frac{\lambda_0}{\lambda} = \frac{C/f_0}{C/f_{zi}} = \frac{f_{zi}}{f_0}$$

Replacing the values of θ_1 and θ_2 in **Equation III.8** gives:

$$k * \tan\left(\theta_{01}\frac{f_{zi}}{f_0}\right) * \tan\left(\theta_{02}\frac{f_{zi}}{f_0}\right) = 1 \qquad (III.10)$$

Equation III.10 represents an equation of three variables. To solve it, a numerical iteration method should be developed. Whether giving values for θ_{01}, θ_{02} and finding k, or giving values for k and θ_{02}, and finding θ_{01} leads to satisfactory results.
Let try the second proposition.

Equation III.10 could be written as:

$$\theta_{01} = \frac{f_0}{f_{zi}} * \arctan\left(\frac{1}{(k * tan\left(\theta_{02}\frac{f_{zi}}{f_0}\right)}\right) \qquad (III.11)$$

Here, a MATLAB program (Appendix A) has been developed to solve the given equation.
By running the program, a bench of results has been obtained. It is presented in **Table III. 1**:

Table III. 1: Results obtained from the developed MATLAB program

k	θ_{02}	θ_{01}	k	θ_{02}	θ_{01}	k	θ_{02}	θ_{01}
1.570	2.050	0.984	2.800	2.280	0.465	**4.750**	**2.320**	**0.266**
1.600	2.070	0.951	3.000	2.290	0.429	5.870	2.330	0.212
1.700	2.120	0.864	3.300	2.300	0.387	5.900	2.330	0.211
1.890	2.180	0.743	3.380	2.300	0.380	6.000	2.330	0.207
1.980	2.200	0.698	3.740	2.310	0.339	6.150	2.330	0.203
2.040	2.210	0.674	3.800	2.310	0.334	6.450	2.330	0.194
2.100	2.220	0.649	3.880	2.310	0.328	6.700	2.330	0.187
2.250	2.240	0.596	4.450	2.320	0.282	6.900	2.330	0.182
2.350	2.250	0.566	4.500	2.320	0.280	7.000	2.330	0.179
2.460	2.260	0.536	4.600	2.320	0.274	7.050	2.330	0.178
2.600	2.270	0.504	4.680	2.320	0.270	7.100	2.330	0.177

Although all the presented results in **Table III. 1** are correct, the best result is selected taking into consideration some criteria and limitations.

For example, if the first result is selected (k = 1.57, θ_{02}= 2.050, θ_{01}= 0.984), the stubs lengths are calculated as follows:

$$k = \frac{Y_1}{Y_2} = \frac{Z_2}{Z_1} = 1.57$$

If Z_1 is selected to be Z_1 = 25 Ohms, then Z_2 = 39.25 Ohm.

Using the LineCalc tool of ADS software, the characteristic impedance and the electrical length for each stub are used to calculate the correspondent length and width.

For Stub1: Z_1 = 25 Ohm, θ_{01}= 0.984 rad = 56.38°,

Figure III. 4 illustrates the LineCalc tool used to obtain the given length and width.

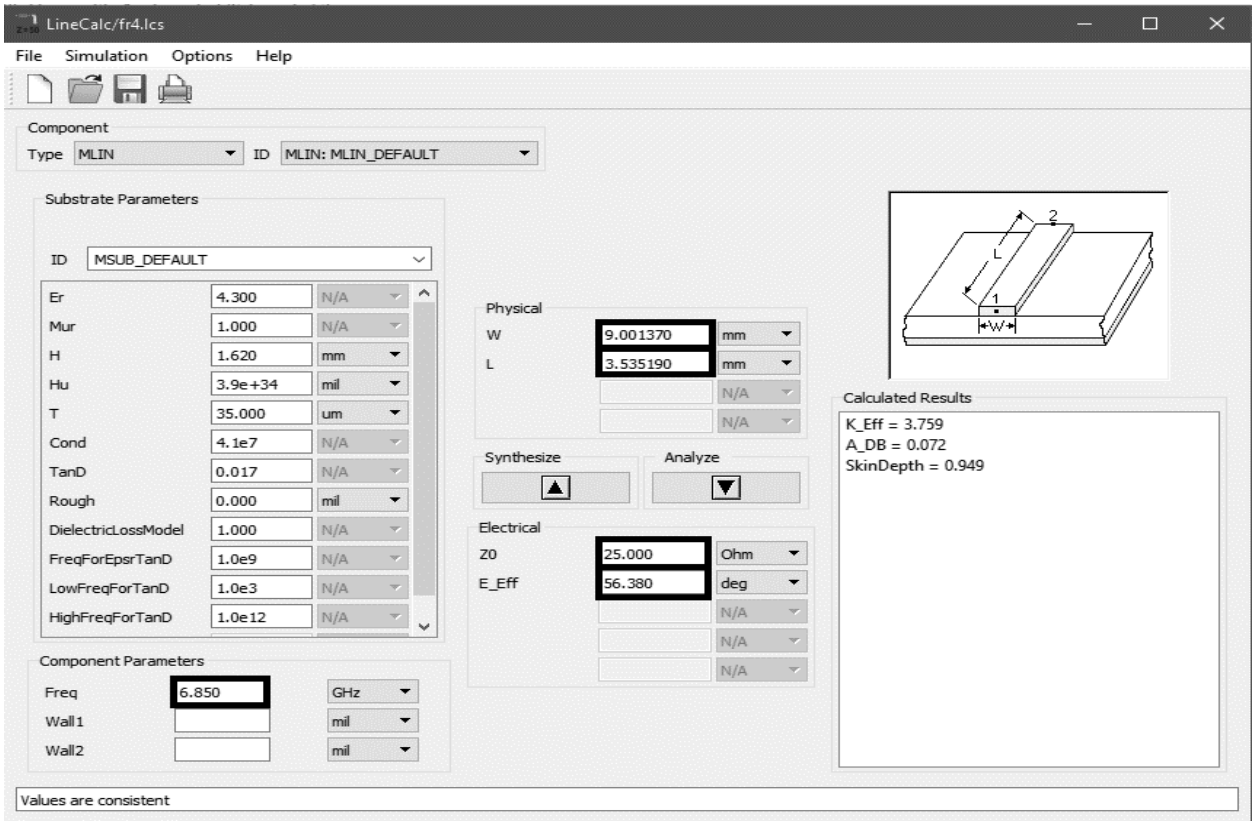

Figure III. 4: LineCalc tool of ADS software, used to calculate the length and the width of the provided stub.

The obtained length and width of stub1 are L_1 = 3.53 mm, W_1 = 9 mm.

Following the same procedure for stub2 (Z_2 =39.25 Ohm, θ_{02}= 2.050 rad = 117.46°), the length and the width are obtained. L_2 = 7.6 mm, W_2 = 4 mm.

By analyzing those results, it is clear that the length (L_1+L_2 = 11.13 mm) is relatively long, and this affects the compactness of the designed filter. Thus, selecting k = 1.57 is not a good choice.

Let investigates the results when the last value of k is selected: k = 7.1.

If Z_1 = 25 Ohms, then Z_2 = 177.5 Ohm, and this exceeds the appropriate range for the characteristic impedance (the width of the line is very small to be fabricated with the available fabrication machines). Thus, selecting k = 7.1 is neither a good choice.

To satisfy both stated conditions, the selected value of k should be in the middle, between the min and the max values. So, the value k = 4.75 may lead to good results in terms of compactness and agreement of characteristic impedance.

For Z1 = 25 Ohms, the characteristic impedance of stub2 would be Z_2 = 118.75 Ohm. This leads to the following values:

For stub1: L_1 = 0.956 mm, W_1 = 9 mm

For stub2: L_2 = 9.52 mm, W_2 = 0.43 mm

Designing the stepped impedance stub with the obtained values is illustrated in **Figure III. 5**.

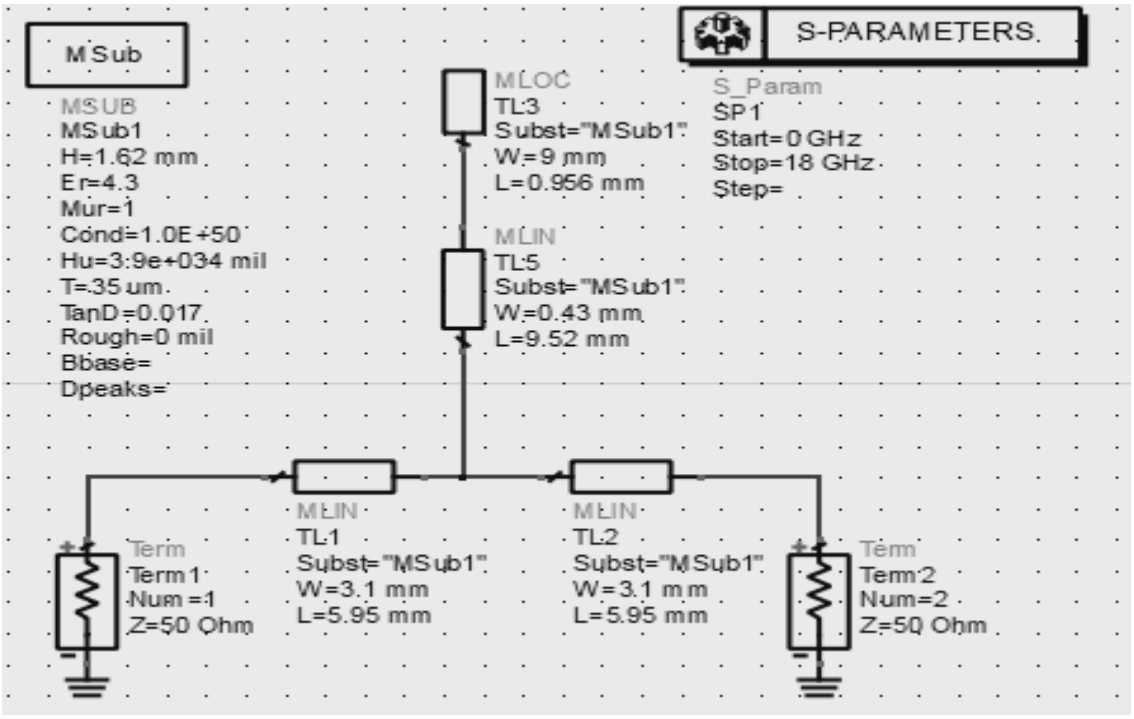

Figure III. 5: ADS Circuit design of the transmission line with the stepped impedance stub.

Simulating the circuit illustrated in **Figure III. 5**, gives the response shown in **Figure III. 6**.

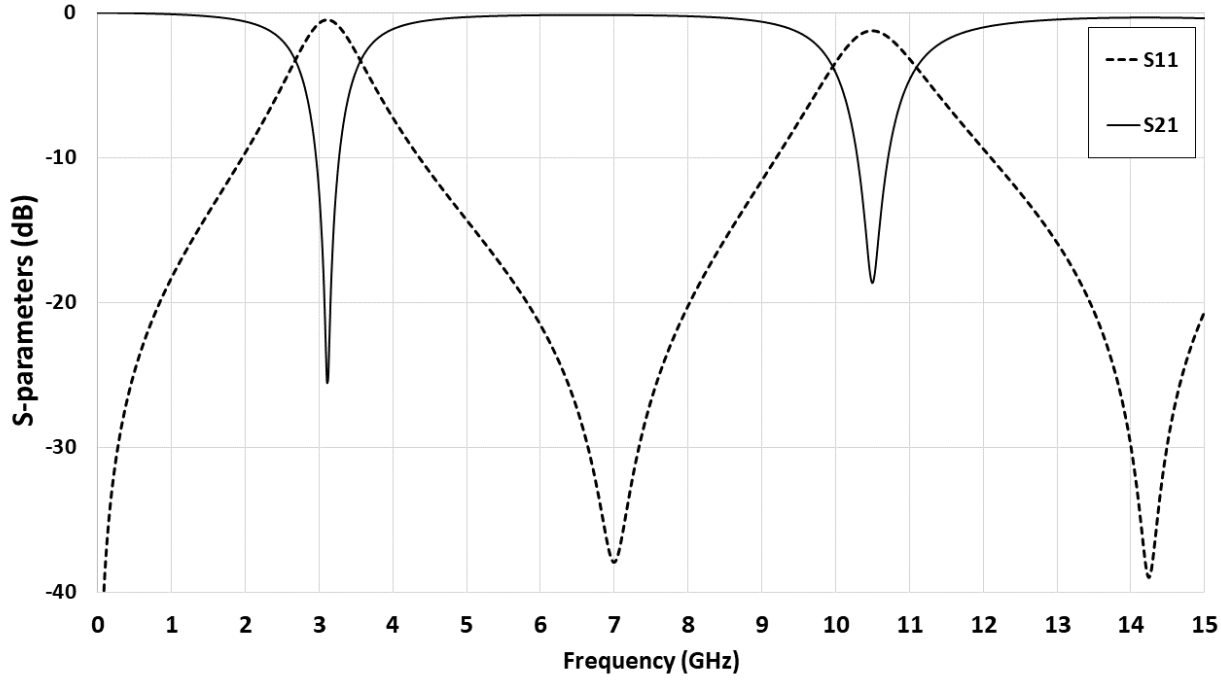

Figure III. 6: S_{11} and S_{21} responses

From the obtained graphs, it is clear that the transmission zeros have been created at the desired frequencies $fz_1 = 3.1\ GHz$ and $fz_2 = 10.6\ GHz$.

The next step is to attenuate the transmission out of the desired band. To do so, interdigital couplers are used [33].

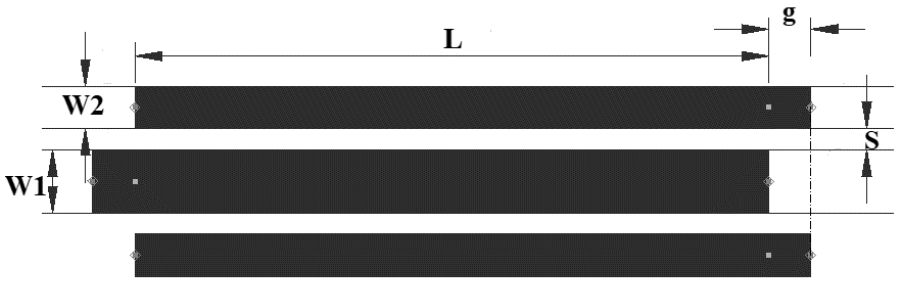

Figure III. 7: Interdigital coupled lines structure

By setting S= 0.2 mm, W1 = 0.6 mm, W2 = 0.4 mm, L = 8 mm, g = 0.2 mm, the electrical simulator of ADS working environment is used to obtain the response of the illustrated interdigital coupler in **Figure III. 8**.

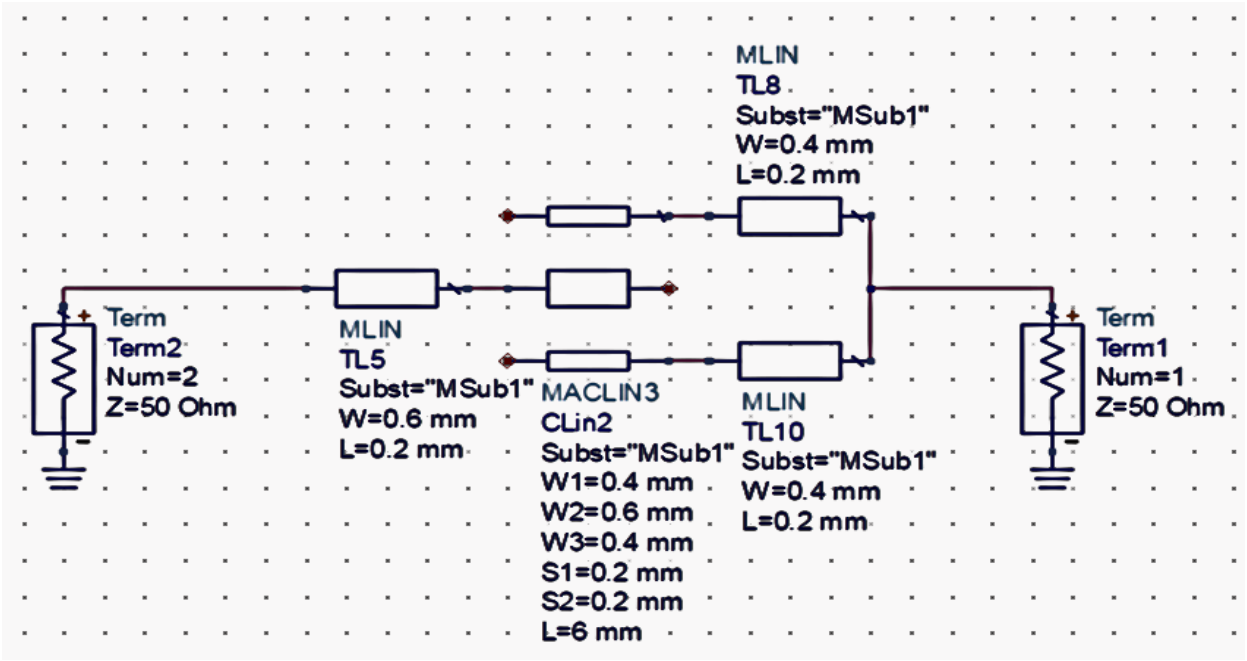

Figure III. 8: Circuit design of interdigital coupler connected to 50 Ohms ports in ADS.

The obtained response is illustrated in **Figure III. 9**.

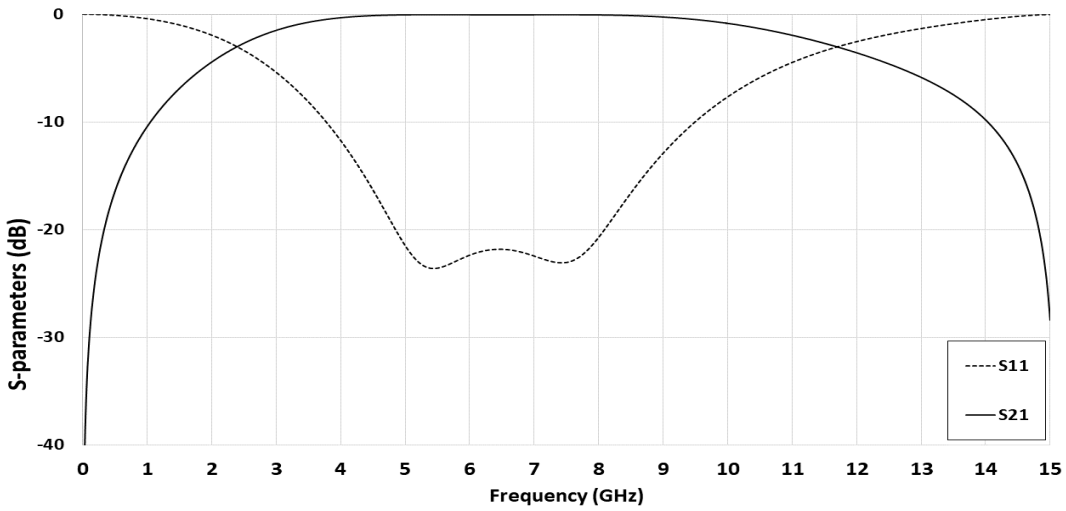

Figure III. 9: S11 and S21 responses of the interdigital coupler

It is clear that the response of the used interdigital couplers attenuates frequencies out of certain band. To match the selected transmission band, tuning procedure to different dimensions should be performed.

The interdigital coupler is added to the circuit illustrated in **Figure III. 5**.

Figure III. 10 represents the new circuit design.

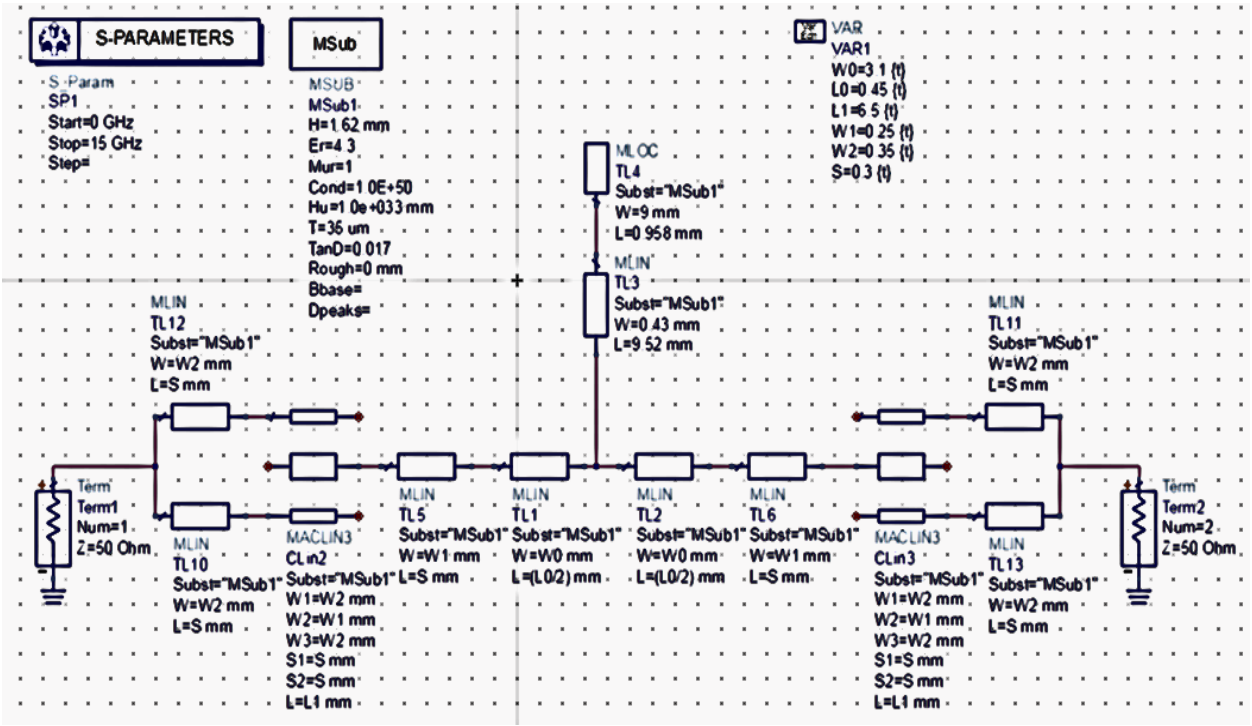

Figure III. 10: Circuit design of the couplers connected to the transmission line with the SIS

Simulating the circuit shown in **Figure III. 10** with the presented parameters gives the responses of S_{11} and S_{21} as shown is **Figure III. 11**.

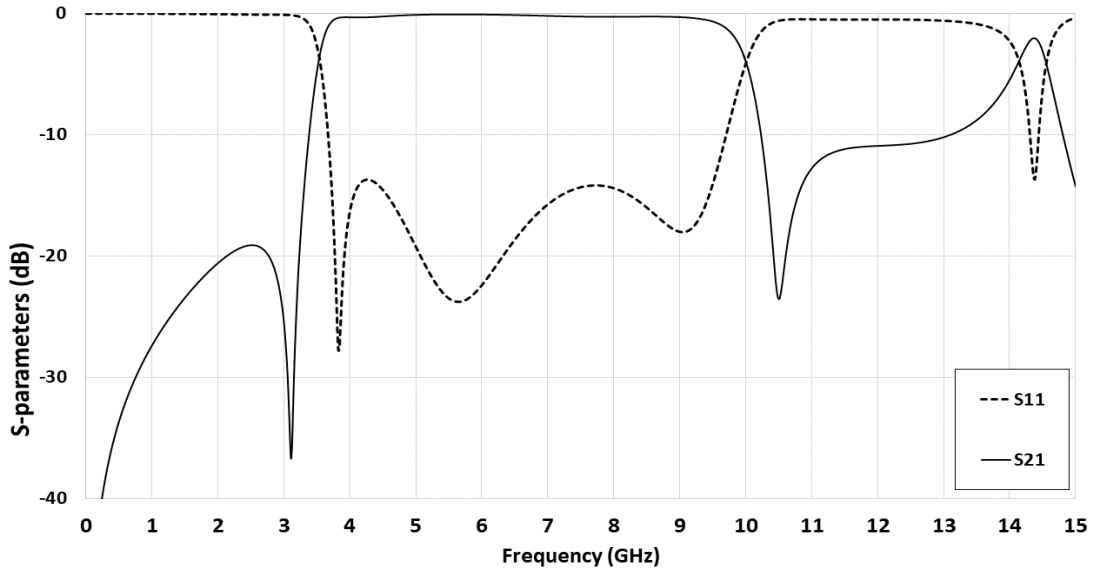

Figure III. 11: S_{11} and S_{22} responses of the designed circuit

From **Figure III. 11**, it can be noticed that the coupled lines have created the out of band rejection, the passband is from f_{C1} = 3.5 GHz to f_{C2}= 10 GHz.

The next step is performing Electromagnetic (EM) simulation after generating the layout in Momentum of ADS software. The generated layout is illustrated in **Figure III. 12**.

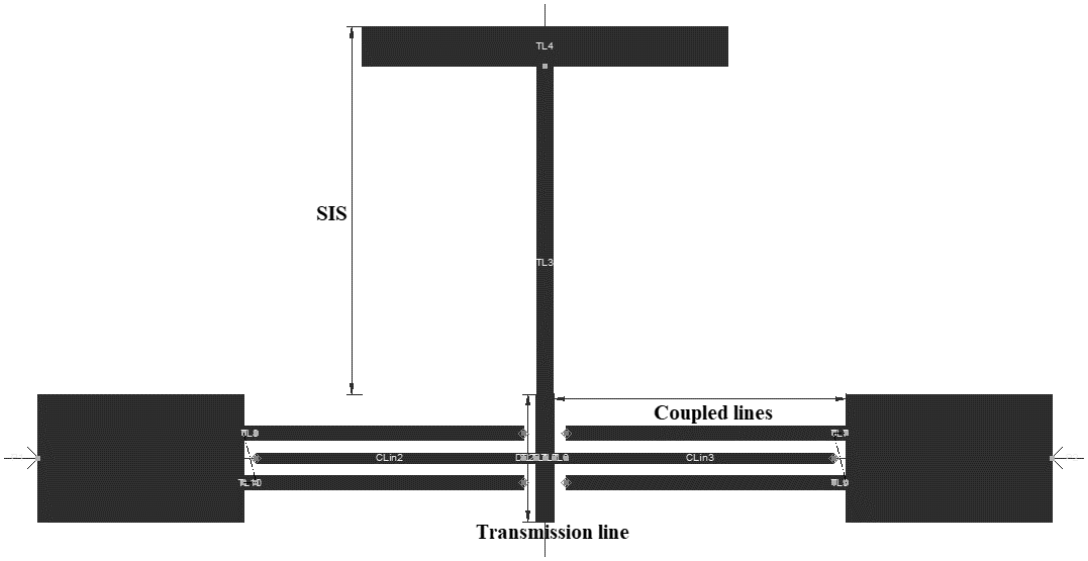

Figure III. 12: Generated layout of the designed filter

Using EM simulator in Momentum, the obtained response is shown in **Figure III. 13**.

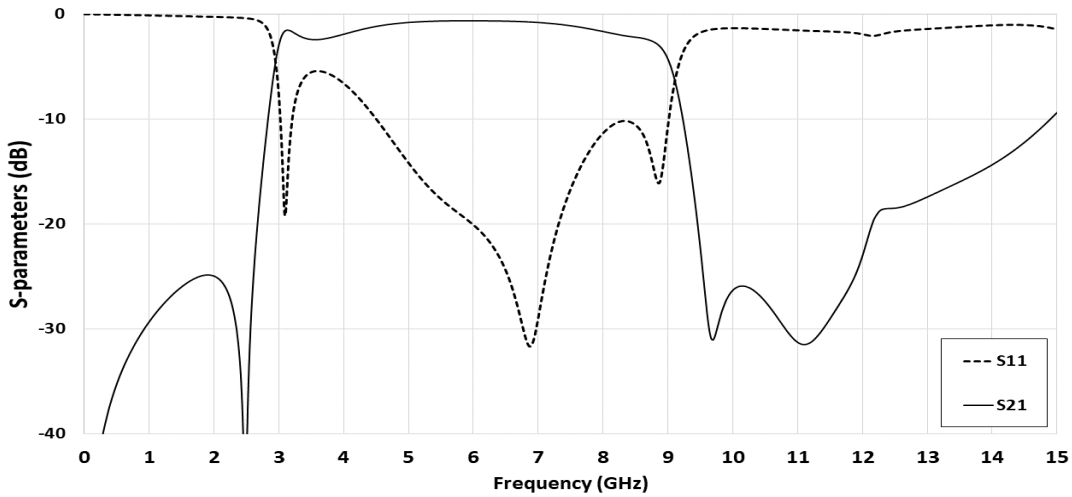

Figure III. 13: EM full-wave simulation of the generated Microstrip structure

Observing the EM simulation in **Figure III. 13**, it can be noticed that the passband is from f_{C1} = 3 GHz to f_{C2}= 9.1 GHZ with deterioration of S_{11} response. To reach the desired band (3.1-10.6 GHz) the SIS dimensions should be modified for the sake of passband enlargement, i.e. the second transmission zero have to be shifted up.

To get the desired passband in EM simulation, it is found after several trials that the transmission zeros could be set to $fz_1 = 2.9\ GHz$ and $fz_2 = 13.7\ GHz$ which can be designed with a SIS having the following dimensions (selecting the following parameter values k = 5.16, θ_{01}= 0.5498 rad, θ_{02}= 1.62 rad, from the results bench):

Stub 1: L1 = 1.97 mm, W1 = 9 mm.

Stub 2: L2 = 6.7 mm, W2 = 0.32 mm.

The new circuit is illustrated in figure **Figure III. 14**.

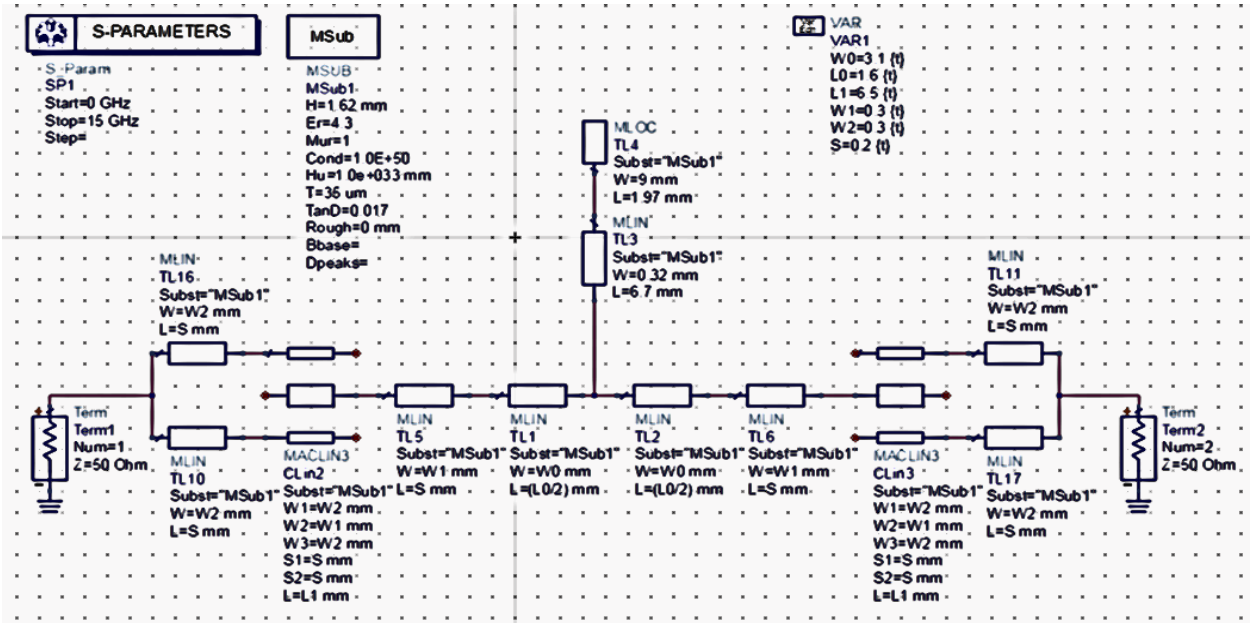

Figure III. 14: ADS circuit with new stub dimensions

The Electric simulation of the circuits shown in **Figure III. 14** is illustrated in **Figure III. 15**.

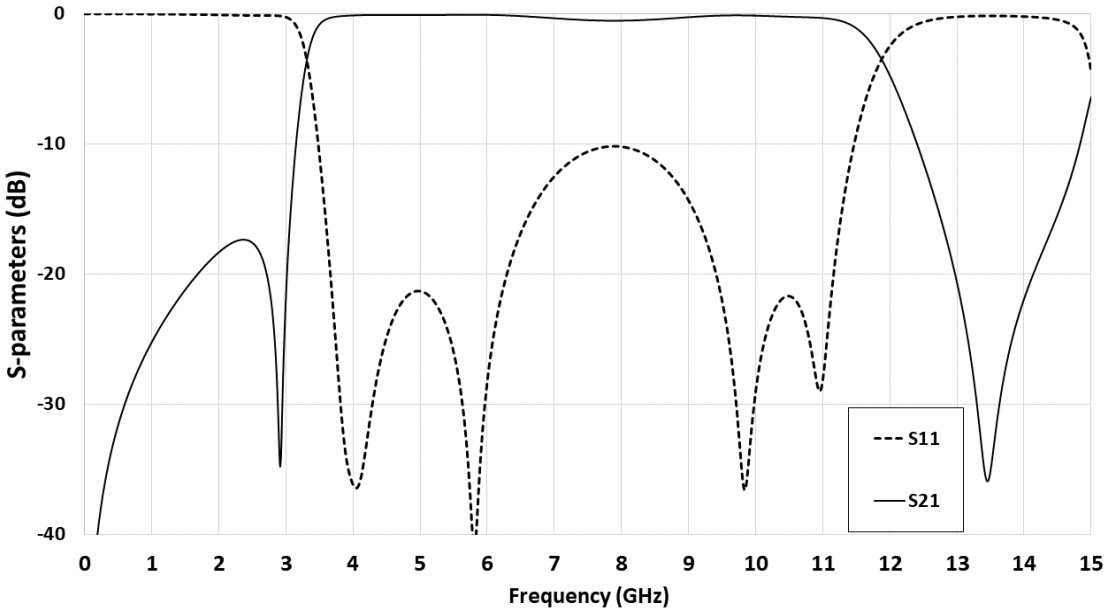

Figure III. 15: Electric simulation of the new designed circuit

From **Figure III. 15** it is clear that the transmission zeros have been set to the mentioned frequencies.

Performing EM full wave simulation to the circuit in **Figure III. 14** gives the response shown in **Figure III. 16**:

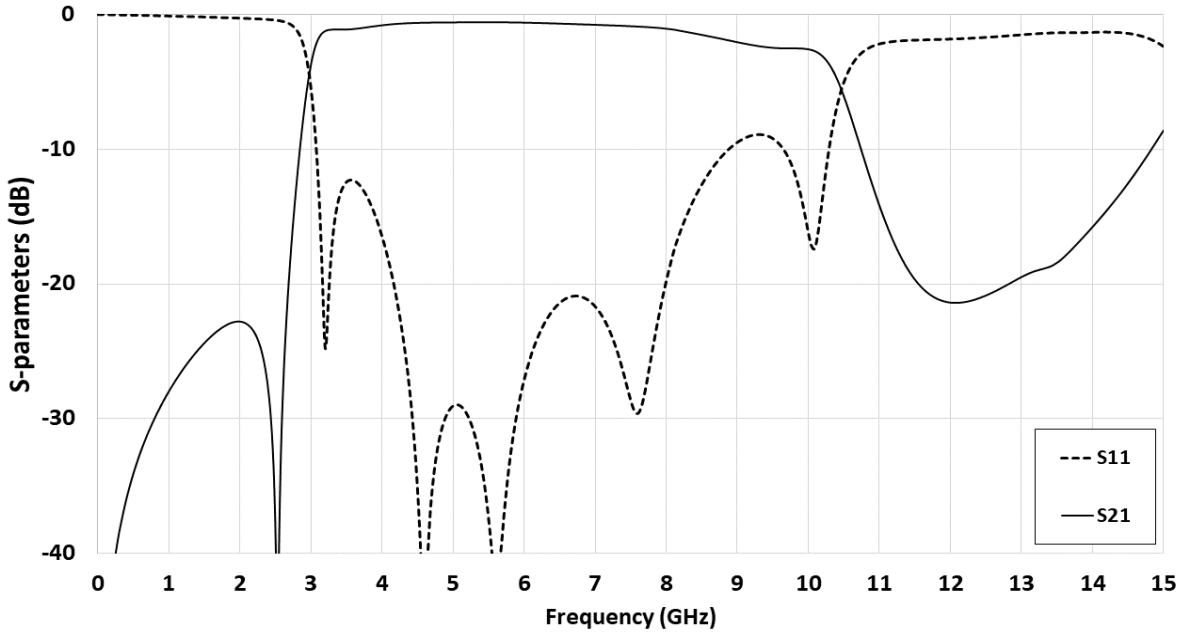

Figure III. 16: EM full wave simulation of the new designed circuit

From **Figure III. 16**, it is noted that the transmission band has been set to the desired one (3.1 - 10.6 GHz).

Now, the next step is to enhance the performance of the designed filter. To do so, CST software has been used for parametric study.

The UWB BPF structure shown in **Figure III. 17** and its simulation have been carried out by using CST software.

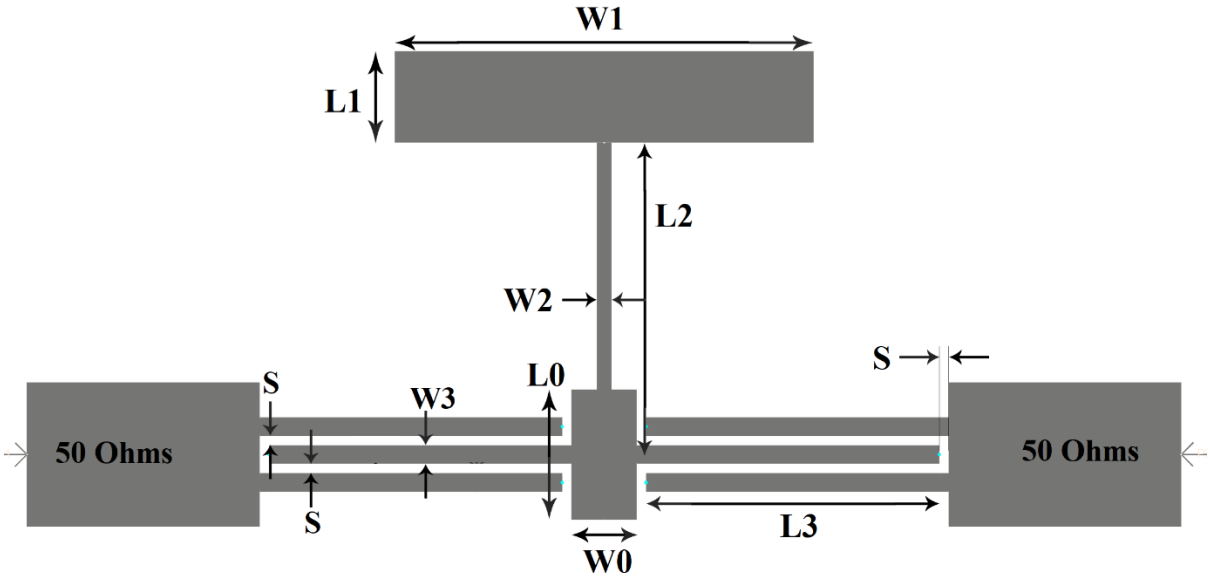

Figure III. 17: UWB Bandpass Filter Structure

The simulation results with the initial parameters presented in **Figure III. 14** and in **Table III. 2** are illustrated in **Figure III. 18**

Table III. 2: Initial parameters of the designed filter structure

Parameter	L0	W0	L1	W1	L2	W2	L3	W3	S
Dimension(mm)	1.6	3.1	1.97	9	6.7	0.32	6.5	0.3	0.2

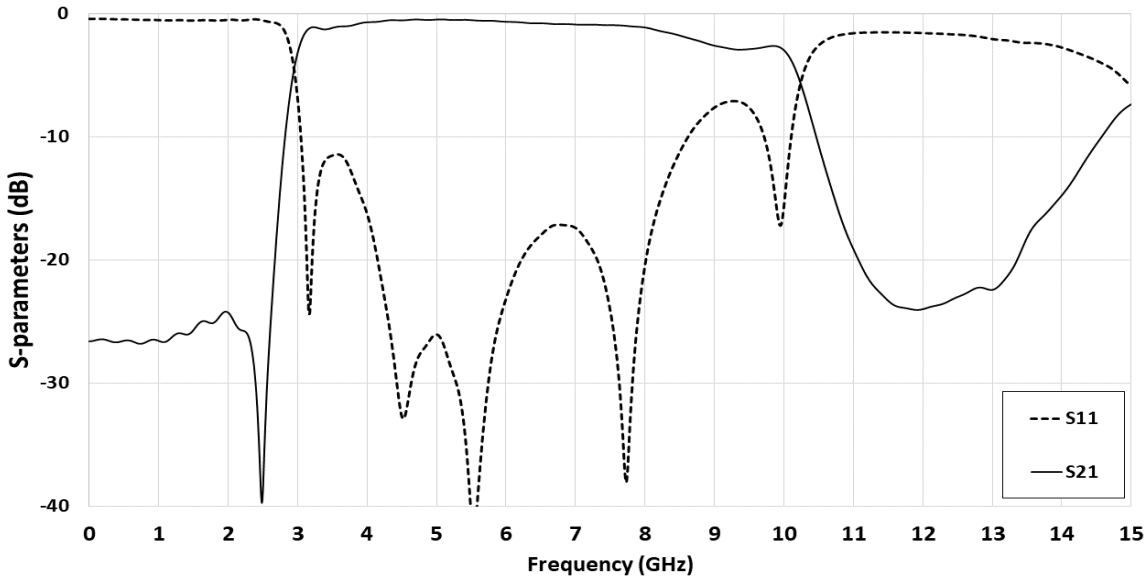

Figure III. 18: CST simulation with the initially presented dimensions of the filter structure

Initially, the required pass band is created. The next step is to enhance the S_{11} response. Investigating the effect of parameters variation, a parametric study is done.

First sweeping L3 from 6.1 mm to 6.7 mm with step of 0.2 mm leads to the results presented in **Figure III. 19**.

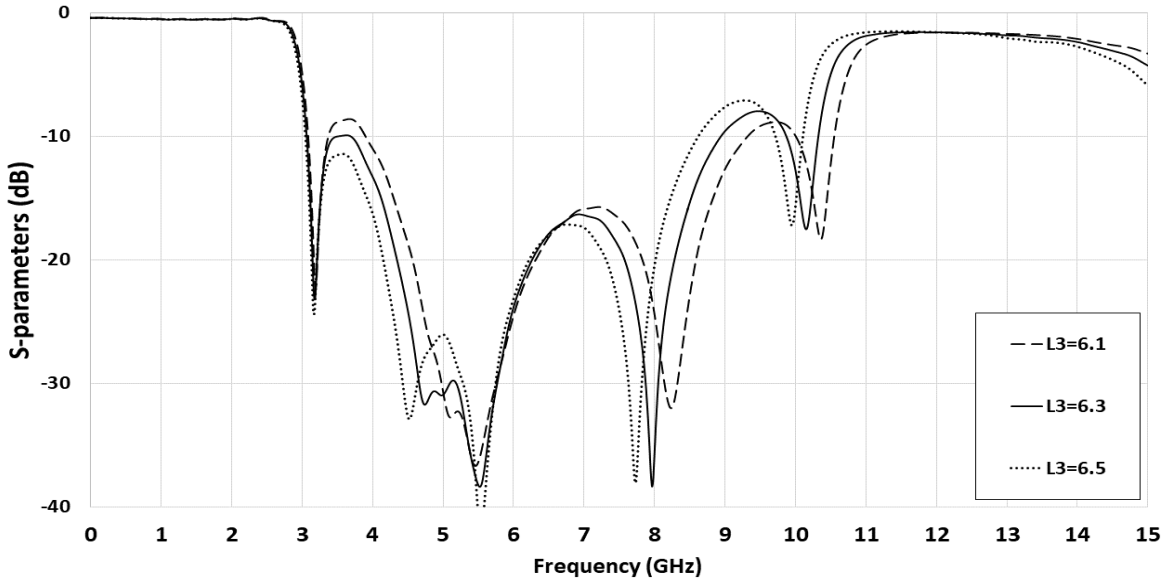

Figure III. 19: Simulated S_{11} with different values of the length L3

Analyzing the obtained results, the curve corresponding to L3 = 6.3 mm is selected, since it has enlarged the pass band to 10.6 GHz, and has made some enhancement to S_{11} response.

For the sake of S_{11} response improvement a rectangular DGS slots are introduced below the couplers [34], having the following initial dimensions: Lg = 4.6 mm, Wg = 1.6 mm, D = 3.25 mm. **Figure III. 20** illustrates the filter structure including the rectangular DGS unit.

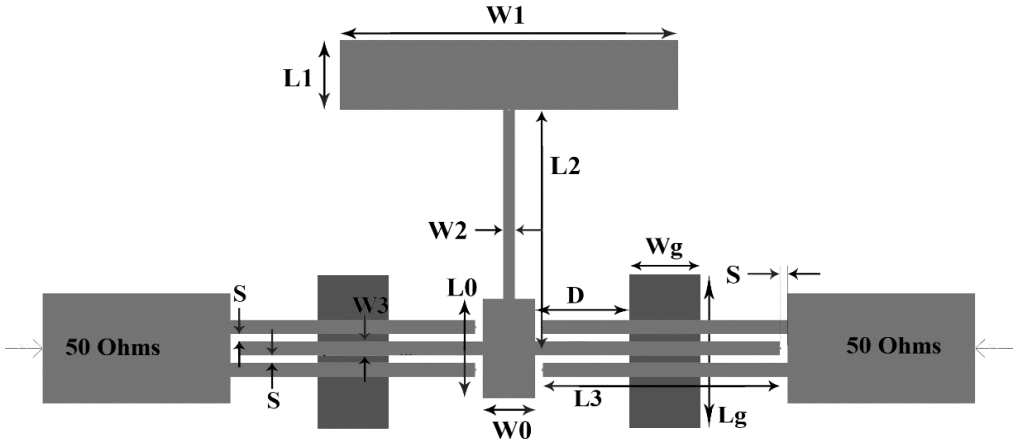

Figure III. 20: Filter structure including rectangular DGS slots

The obtained simulation after adding the rectangular DGS units is illustrated in **Figure III. 21**.

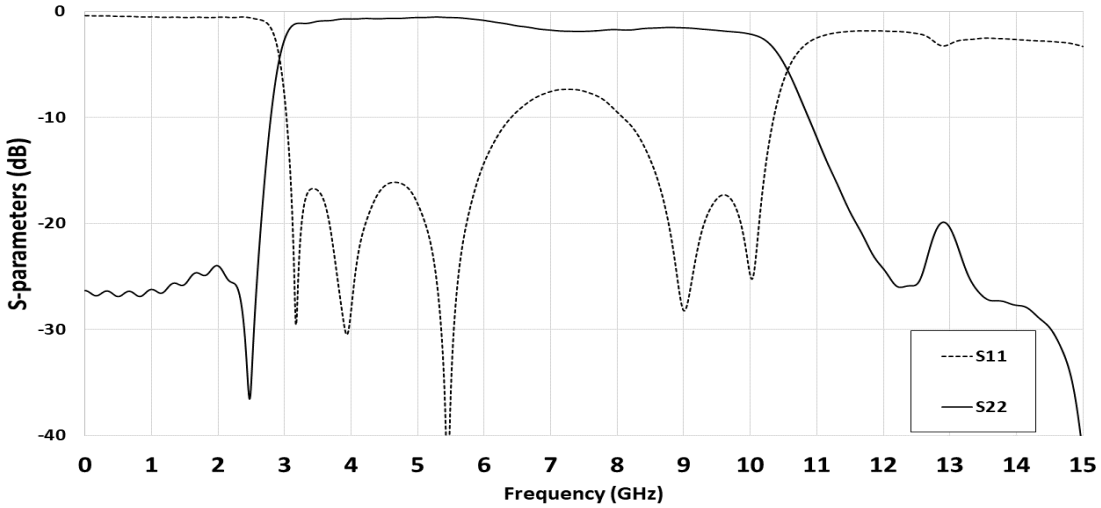

Figure III. 21: EM full wave simulation of the designed UWB BPF filter with DGS

As expected, the inserted DGS had improved the S_{11} performance. As it is observed, the most right and left ripples reached the –15 dB level, but another problem is encountered. One of the middle ripples raised to -7 dB level.

To solve the problem, a parametric study to the remaining unchanged parameters is done. First, a sweep of the length L0 is performed from 1 mm to 1.8 mm with 0.4 mm step. **Figure III. 22** presents the obtained results.

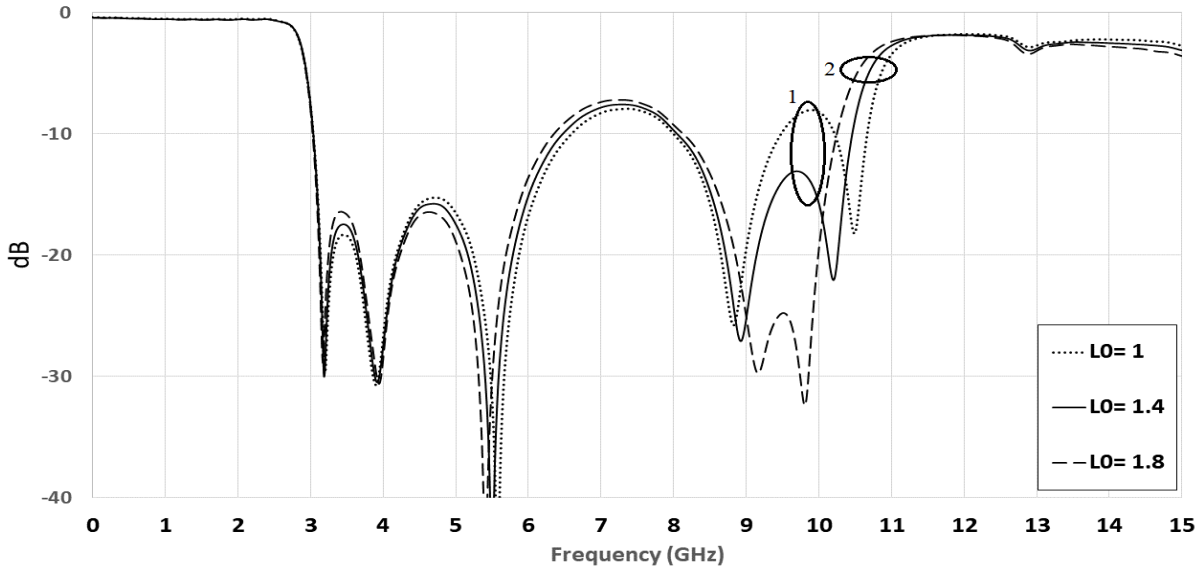

Figure III. 22: Parametric study of the length L0

The curve corresponding to L0 = 1.4 mm is selected since it represents a good S_{11} response compared to the curve of L0 = 1 mm (Circle 1), and possesses larger passband than the curve of L0 = 1.8 mm (Circle 2).

The next step is sweeping the coupler width W3 from 0.3 mm to 0.6 mm with a step of 0.15 mm. **Figure III. 23** shows the obtained results.

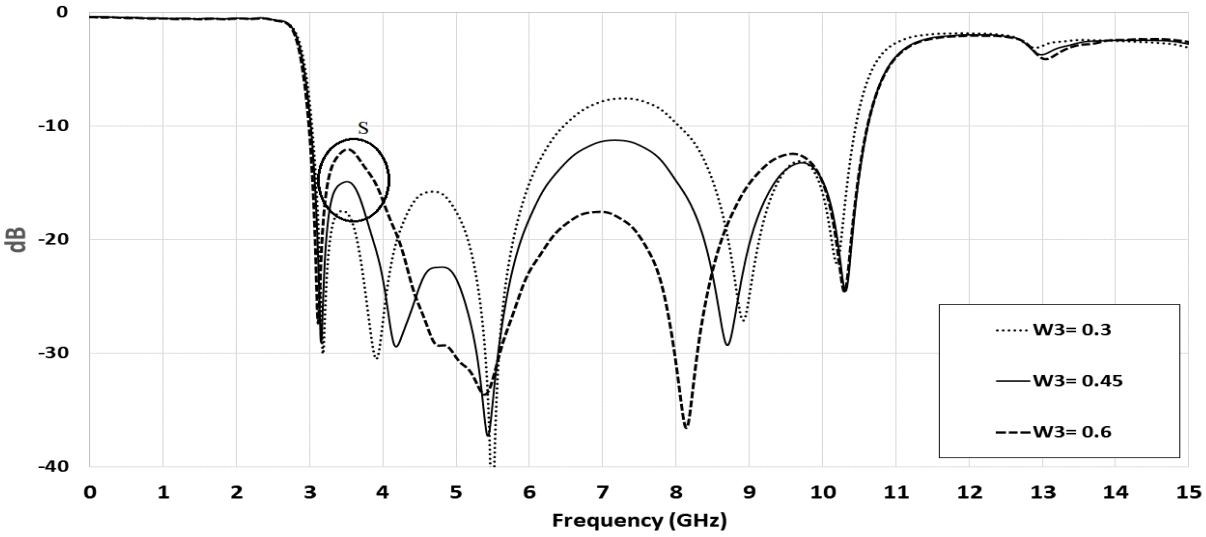

Figure III. 23: Parametric sweep of the coupler width W3

Observing **Figure III. 23**, it is noticed that the most left ripple of S_{11} response reaches the -15 dB level with the curve corresponding to W3 = 0.45 mm (Circle S). To keep this ripple below -15 dB level, the curve corresponding to W3 = 0.45 mm is selected.

The last unchanged parameter in the filter structure (excluding DGS parameters) is the width W0. Let investigate its variation effect. The parametric sweep is done from 2.5 mm to 3.1 mm with a step of 0.3 mm. the results are illustrated in **Figure III. 24**.

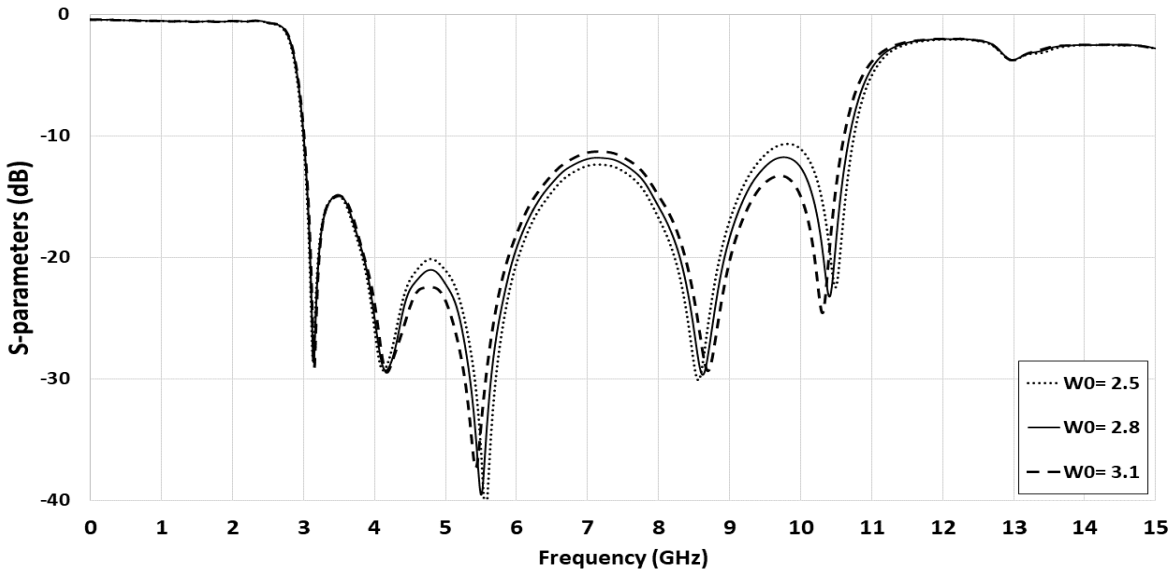

Figure III. 24: Parametric study of the width W0

From the obtained results illustrated in **Figure III. 24**, it is observed that the curve corresponding to the width W0 = 2.8 mm possesses the best S_{11} response. Thus, the width W0 = 2.8 mm is selected.

Now, let investigate the effect of varying DGS parameters.

First, let start by varying the distance D illustrated in **Figure III. 20**.

A distance sweep is done from 1.85 mm to 3.25 mm. the result is shown in **Figure III. 25**

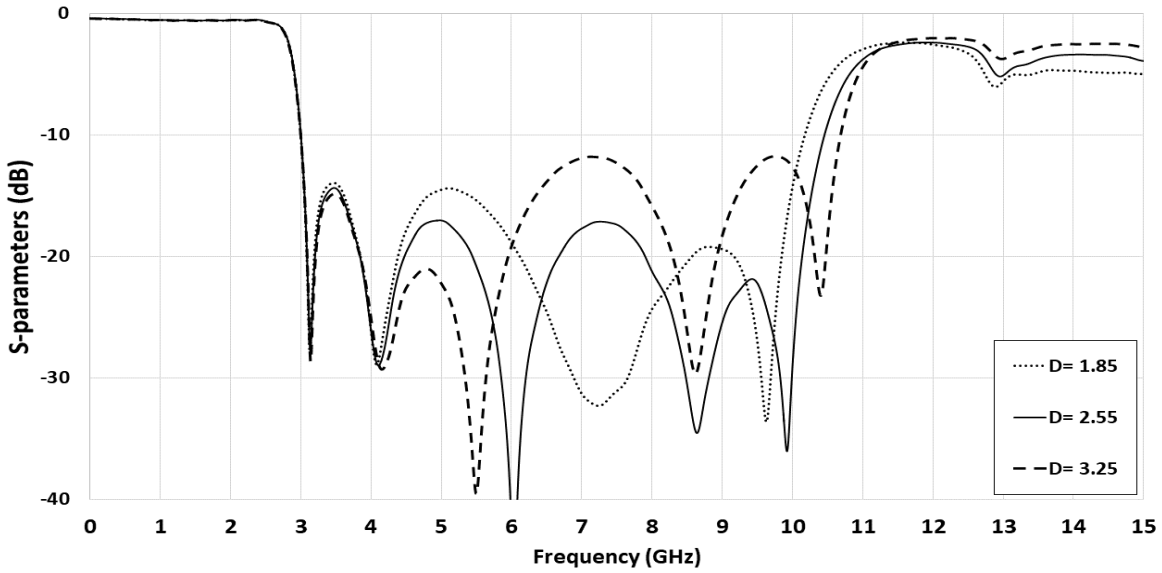

Figure III. 25: Parametric sweep of the distance D

It is clear that the curve corresponding to D = 2.55 mm presents good S_{11} response (below - 15 dB level), and wider band compared to the curve corresponding to D = 1.85 mm. So, the parameter D is selected to be D = 2.55 mm.

Second, the rectangular DGS slot length Lg is varied from 4.2 mm to 5 mm.

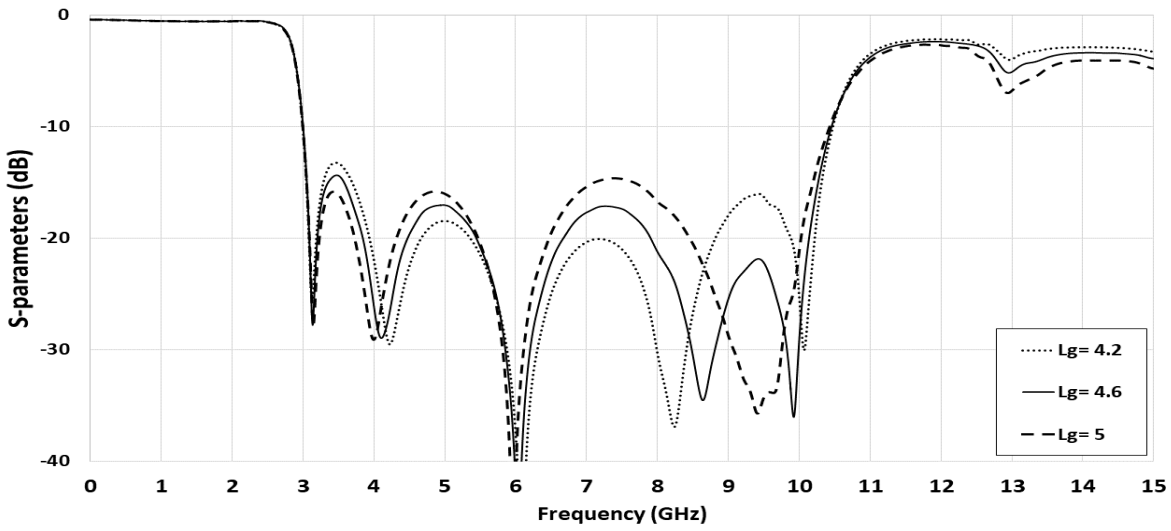

Figure III. 26: Parametric sweep of the rectangular DGS slot length Lg

The curve corresponding to Lg = 4.6 mm is selected since it represents the best S_{11} response (below -15 dB level) from the presented graphs in **Figure III. 26**.

Finally, let see the effect of varying the rectangular DGS slot width Wg. The range (1.2 – 2) mm is selected for the parametric study with step of 0.4 mm. **Figure III. 27** shows the obtained graphs.

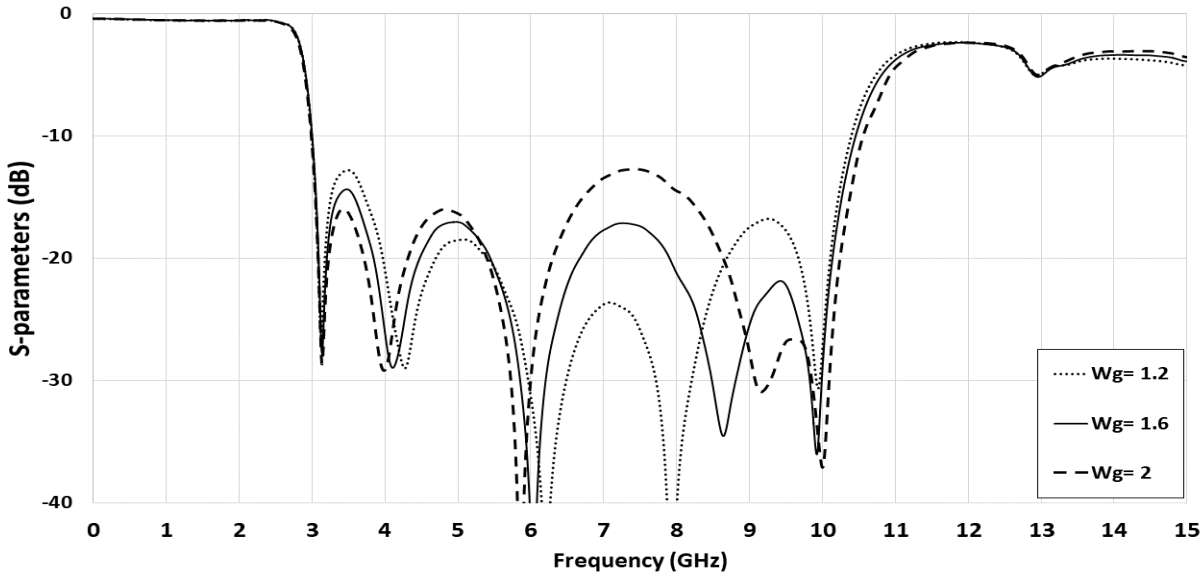

Figure III. 27: Parametric sweep of the rectangular DGS slot width Wg

The curve corresponding to Wg = 1.6 mm is selected since it represents the best S_{11} response (below -15 dB level) from the presented graphs.

The final dimensions of the proposed UWB BPF is presented in **Table III. 3**

Table III. 3: Final dimensions of the proposed UWB BPF

Parameter	**L0**	**W0**	**L1**	**W1**	**L2**	**W2**	**L3**	**W3**	**S**	**D**	**Lg**	**Wg**
Dimension(mm)	1.4	2.8	6.7	0.32	6.3	1.97	6.3	0.45	0.2	2.55	4.6	1.6

The final structure of the proposed UWB BPF with the final dimensions has been simulated using EM simulator of CST software. The simulation results of S_{11} and S_{21} are illustrated in **Figure III. 28**.

The obtained simulation presents satisfactory results. An Ultra-wide pass band of 7.7 GHz (2.9 - 10.6 GHz) with a fractional bandwidth of 118.8 %. A return loss better than 15 dB and a sharp selectivity in addition to the wide upper band reject up to 17 GHz.

Since the used substrate is the commercial FR4 substrate with $\mathcal{E}r = 4.3$ which produces more losses because of the high radiation that increases the insertion loss, an IL = 1.5 dB has been obtained.

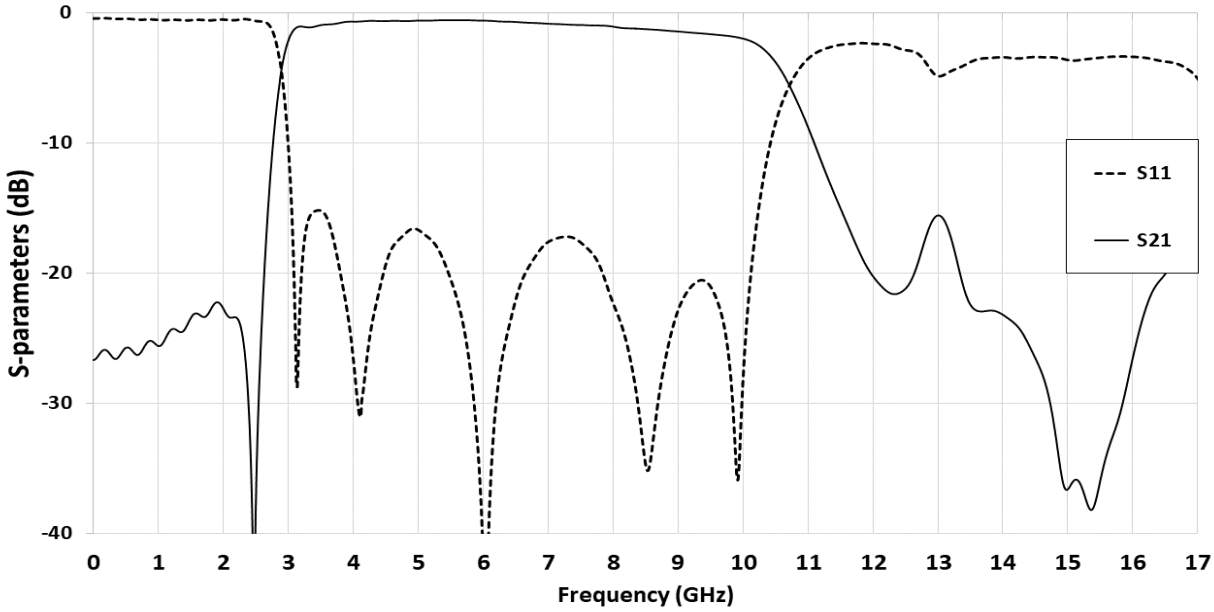

Figure III. 28: S_{11} and S_{21} responses of the final structure of the proposed UWB BPF

To perceive the filter characteristics further, the current density distribution on the proposed UWB bandpass filter is investigated at the central passband frequency 6.85GHz, and at two stop band frequencies 2.5 GHz and 12 GHz. From **Figure III. 29**-(b), it can be observed that Current density is mainly concentrated on the coupled lines. This is due to the presence of rectangular DGS units blow the couplers which provides good coupling. In addition to that, both ports indicate significant current density which may be explained by the fact the frequency 6.85 GHz is inside the pass band, so the signal passes from the input port to the output port.

However, in **Figure III. 29**-(a) and **Figure III. 29**-(c) current density is mainly concentrated at the left part of the structure, which indicates that there is no current flow from port 1 to port 2 at the two stop band frequencies 2.5 GHz and 12 GHz. Another thing to be demonstrated, looking to **Figure III. 28**, a transmission zero is created at 2.5 GHz which means that at this frequency the current is shorted out through the stub. **Figure III. 29**-(a) show strong current density at the stub level which proves the stub function.

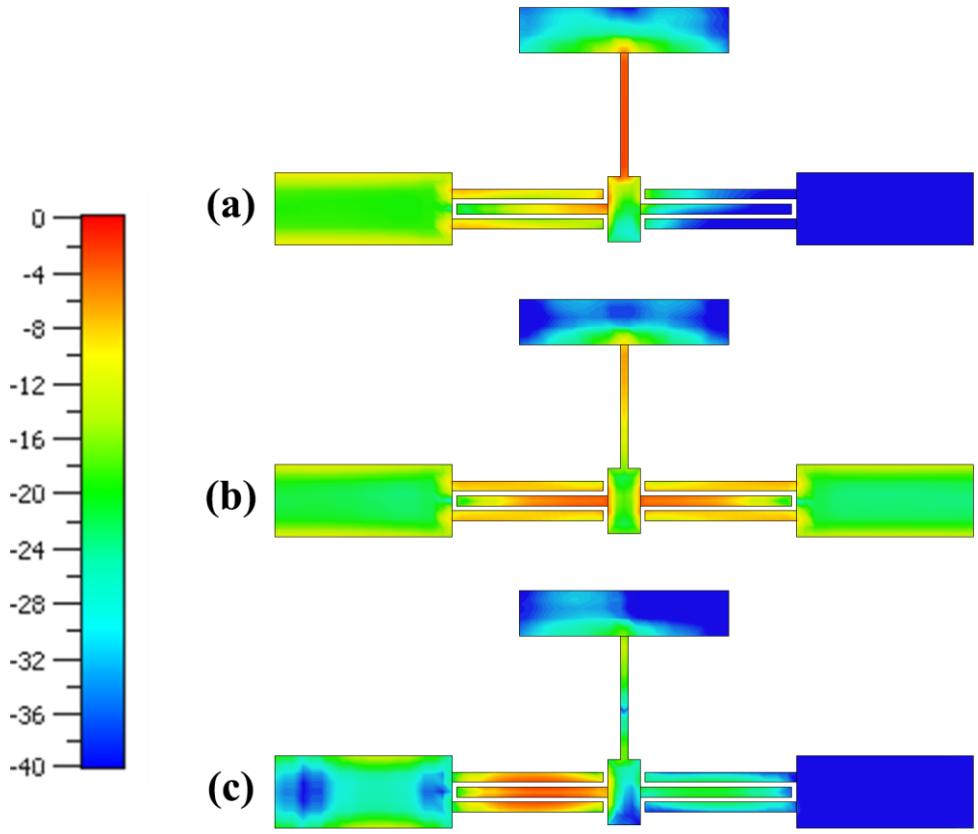

Figure III. 29: Current distribution of the proposed UWB BPF at a) 2.5 GHz; b) 6.85 GHz; c) 12 GHz

3.3 Dual notched band implementation of the proposed UWB BPF

The interference with coexisting wireless communication systems can degrade the performance of UWB systems. The challenging task of UWB is to eliminate the interference with coexisting wireless communication systems. Some of the coexisting communication systems are WiMAX and satellite communication systems, and the operating frequencies are 5.8 GHz and 8.0 GHz [35]. To eliminate interference with coexisting wireless communication systems, ultra-wideband band pass filters with notches are designed. In context, several approaches have been proposed to design UWB BPF with notches [8] [29] [30] [31] [35]. In this work, the notched bands are designed using U-shaped DGS units [36] [37].

The form of the U-shaped DGS unit is illustrated in **Figure III. 30**

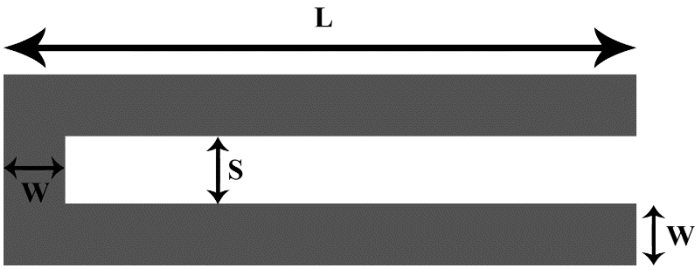

Figure III. 30: U-shaped DGS unit

3.3.1 Design of the first notched band

To design the first notched band, the DGS structure in **Figure III. 30** is introduced to the filter structure as illustrated in **Figure III. 31** with the following initial dimensions: L4 = 7.5 mm, W4= 1 mm, S1= 0.6 mm, and g = 0.35 mm.

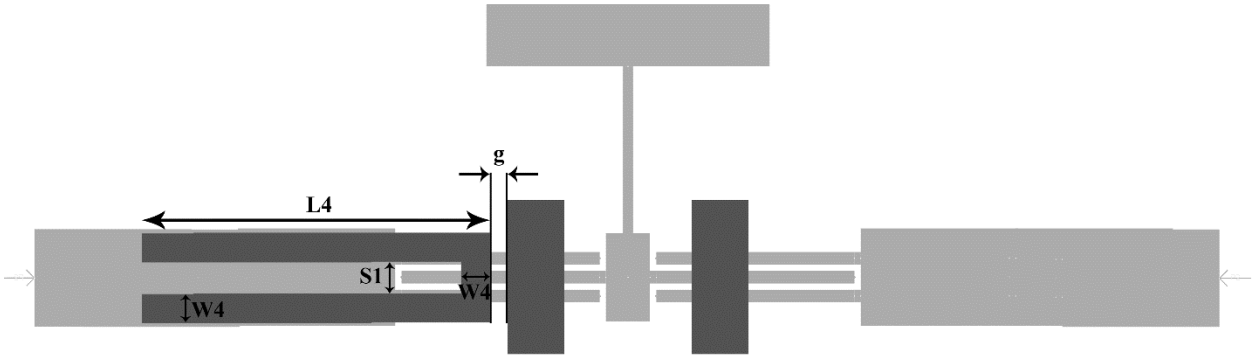

Figure III. 31: Filter structure including the first U-shaped DGS unit

Simulating the structure in **Figure III. 31** gives the response illustrated in **Figure III. 32**.

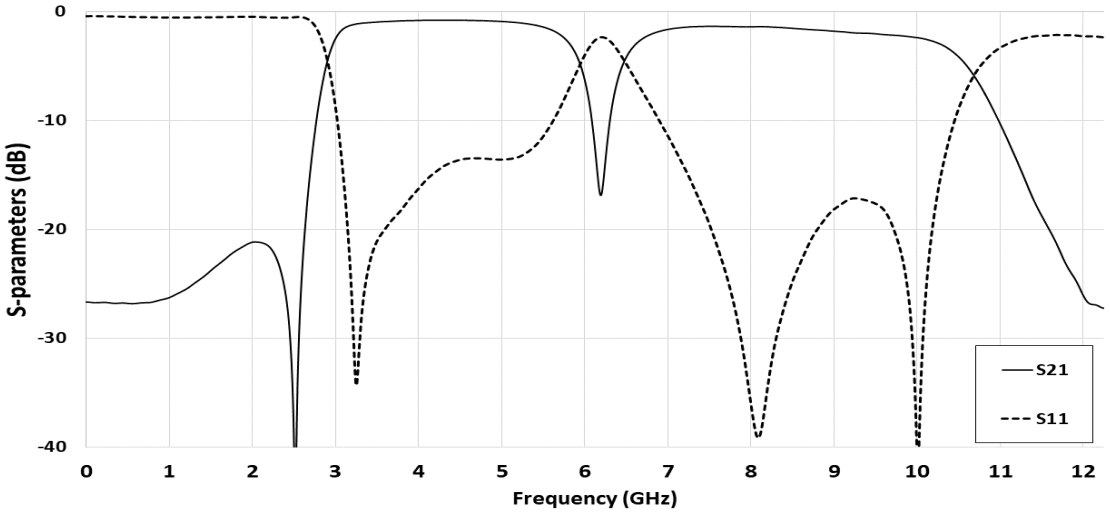

Figure III. 32: UWB BPF response with single notch

As shown in **Figure III. 32**, inserting a U-shaped DGS unit to the filter structure with the stated initial dimensions has created a rejection band at frequency 6.2 GHz.

To reach the desired notch band 5.8 GHz which eliminates WiMAX interference, a parametric study to the dimensions L4, W4 and S1 has been carried out.

First, starting by sweeping the length L4 while keeping the other parameters constant. The obtained results are shown in **Figure III. 33**.

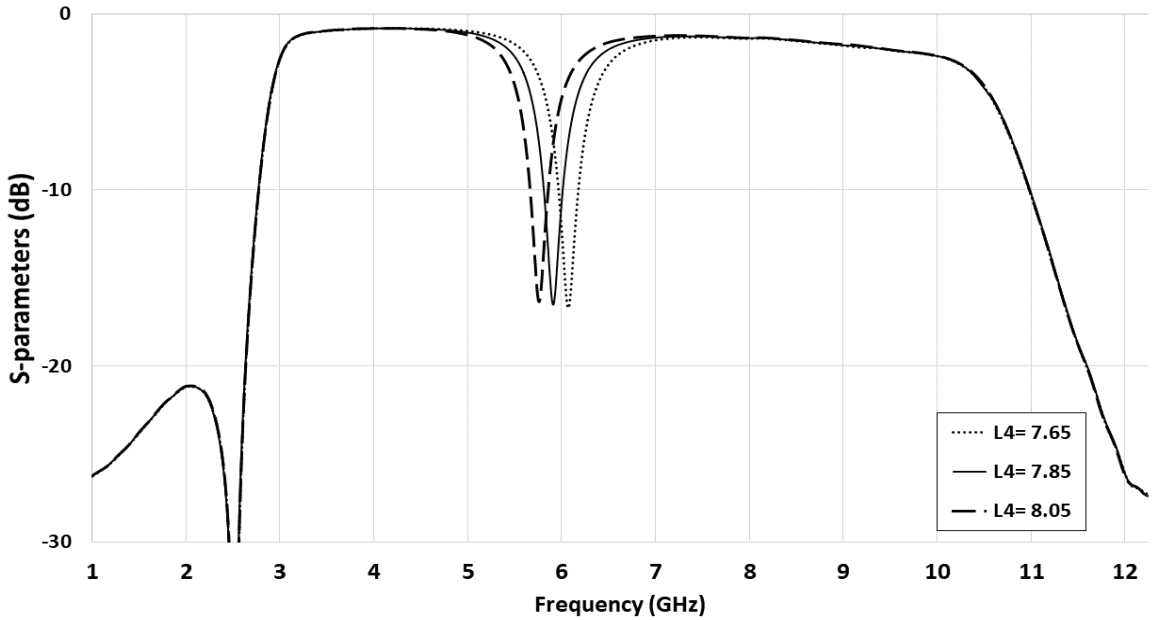

Figure III. 33: S_{21} response resulting from the Parametric sweep of the length L4

It is observed that increasing the length L4 shift the notched band to lower frequencies. As it is noticed, to create the rejection band at 5.8 GHz the length L4 = 7.85 mm should be selected.

Then, varying the width W4 leads to results illustrated in **Figure III. 34**.

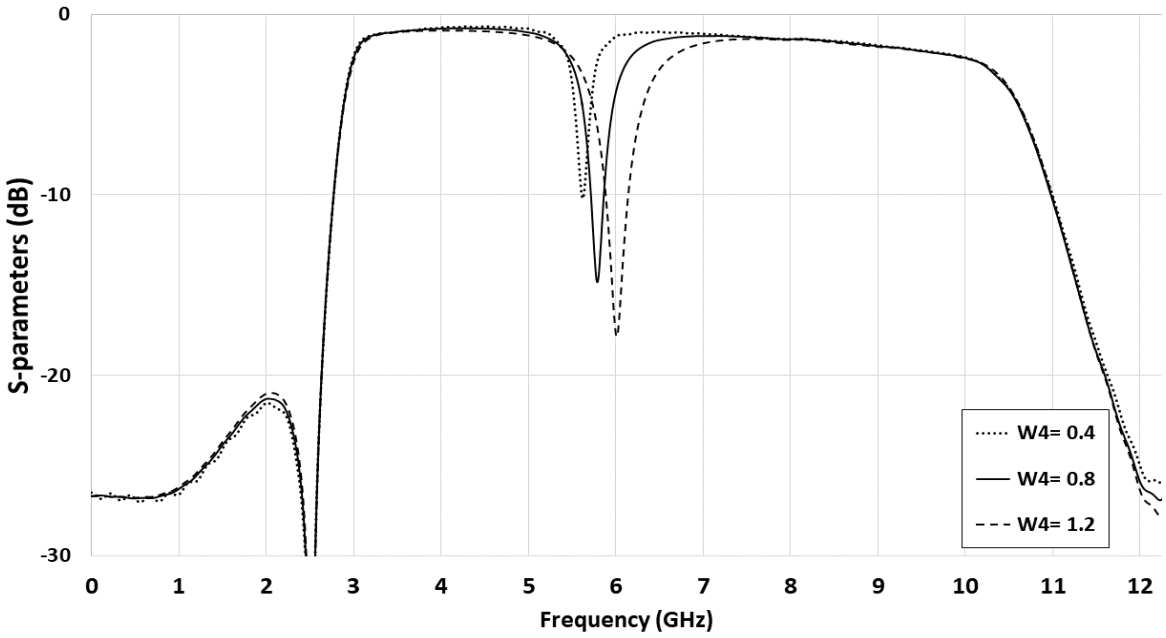

Figure III. 34: S_{21} response resulting from the Parametric sweep of the Width W4

As shown in **Figure III. 34**, it is demonstrated that increasing the width W4 leads to better S_{21} response at the frequency where the notch is created as it reaches -18 dB for W4 = 1.2 mm. But, in reverse, the bandwidth of the created notched band increases which may not lead to better results in terms of the narrowness of the band and the fractional bandwidth. For a good agreement between the two stated propositions, the width W4 = 0.8 mm is selected. The corresponding S_{21} response reaches -15 dB level at the desired band rejection frequency, and possesses a good fractional bandwidth of 3.45 %.

Finally, performing a parametric study to the gap S1 while keeping the other parameters constant leads to the results show in **Figure III. 35**.

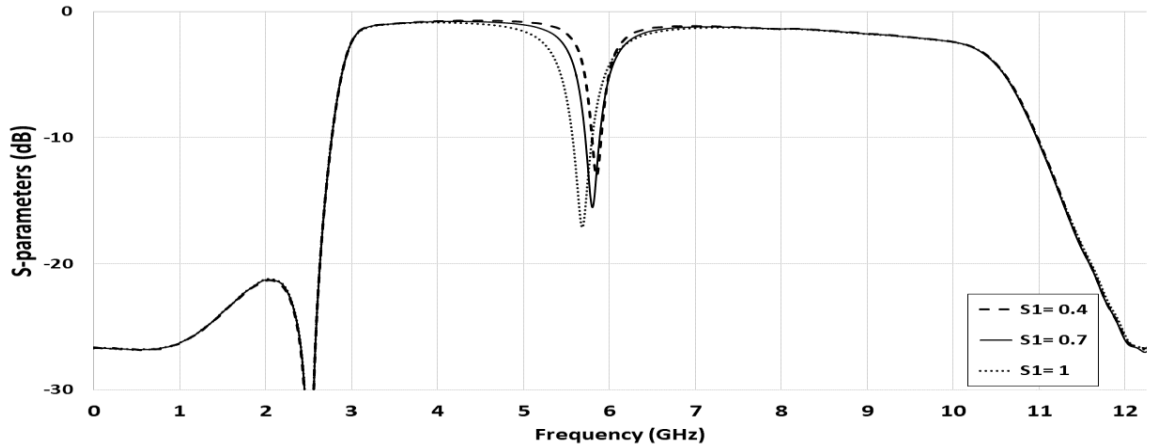

Figure III. 35: S_{21} response resulting from the Parametric sweep of the gap S1

As observed in **Figure III. 35**, it is noticed that varying the gap S1 has the same effect in terms of band enlargement and rejection response enhancement as varying the width W4. So, for the same considered reasons for selecting W4, the gap S1 is selected to be S1 = 0.7 mm.

By performing a parametric sweep to the gap g between the U-shaped DGS unit and the rectangular DGS slot, it is found that it has no effect on the obtained results. For fabrication limitation, it should not be inferior than 0.2 mm. It is selected to be 0.35 mm.

The final dimensions of the created notched band are illustrated in **Table III. 4**

Table III. 4: Final dimensions of the first U-shaped DGS unit

Parameters	**L4**	**W4**	**S1**	**g**
Dimensions(mm)	7.85	0.8	0.7	0.35

The final obtained response is illustrated in **Figure III. 36**

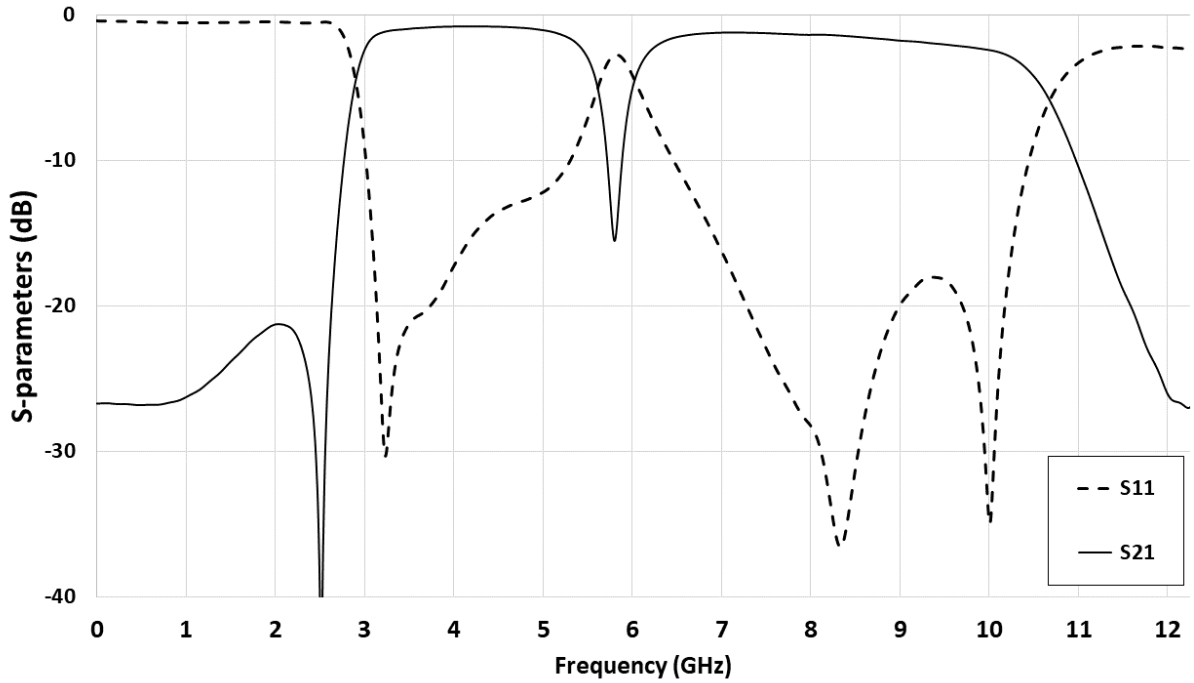

Figure III. 36: S_{11} and S_{21} responses of the designed UWB BPF with single notch

Figure III. 36 illustrates the UWB BPF with single notch EM full wave CST simulation. As observed, the obtained response possesses a pass band 2.9 – 10.6 GHz with a return loss better than 18 dB. the rejection band has a fractional bandwidth of 2.58 %, its rejection reaches -15 dB.

3.3.2 Design of the dual notched band

The second notched band is designed to eliminate satellite communication interference at 8 GHz.

The final structure of the UWB BPF with the dual notched band is illustrated in **Figure III. 37**.

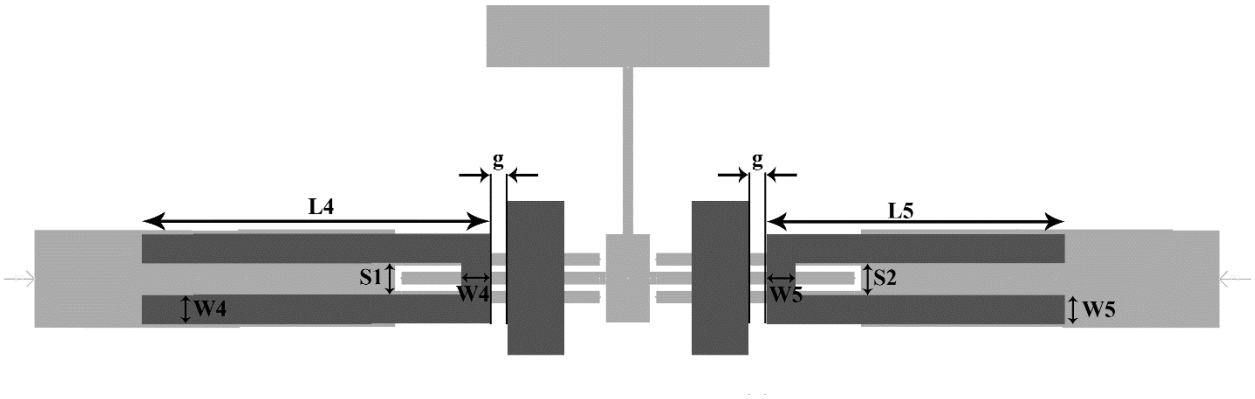

Figure III. 37: Final structure with dual notched band of the UWB BPF

Following the same procedures done for the first notched band implementation, the final dimensions of the second notch have been obtained. **Table III. 5** shows the obtained results.

Table III. 5: Final dimensions of the second U-shaped DGS unit

Parameters	**L5**	**W5**	**S2**	**g**
Dimensions(mm)	5.67	0.8	0.75	0.35

The simulation results are illustrated in **Figure III. 38**.

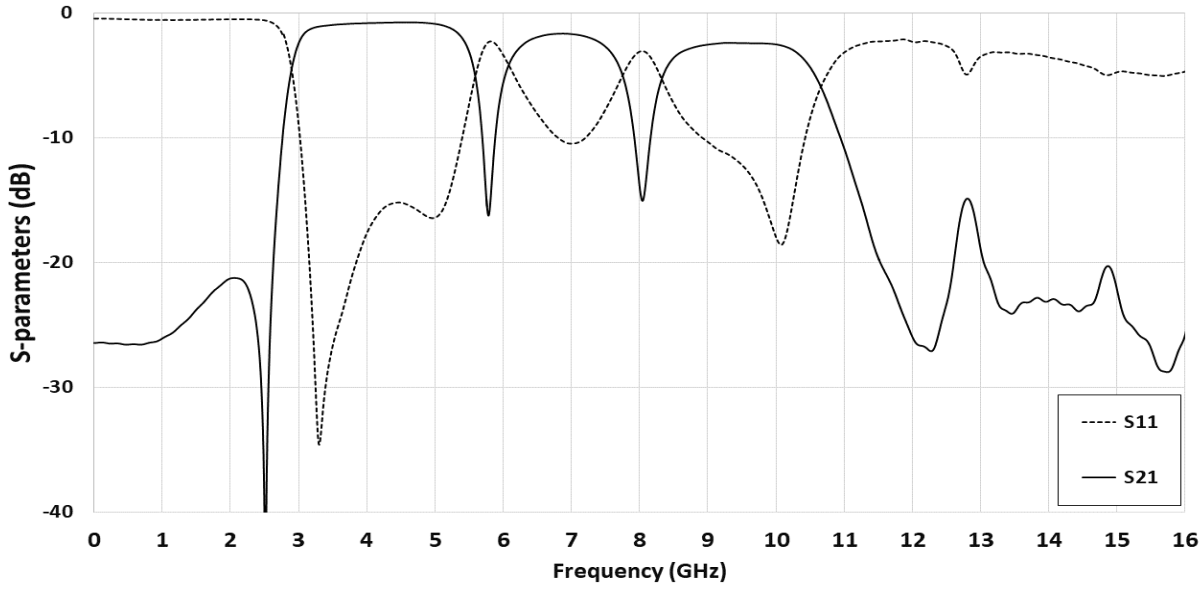

Figure III. 38: Final response of the designed dual notched UWB BPF

The final parameters of the designed filter are presented in **Table III. 6**

Table III. 6: Final design parameters of the proposed UWB BPF with dual notched band

Parameter	**L0**	**W0**	**L1**	**W1**	**L2**	**W2**	**L3**	**W3**	**S**	**D**	**Lg**	**Wg**
Dimension(mm)	1.4	2.8	6.7	0.32	6.3	1.97	6.3	0.45	0.2	2.55	4.6	1.6
Parameter	**L4**	**W4**	**S1**	**L5**	**W5**	**S2**	**g**					
Dimension(mm)	7.85	0.8	0.7	5.67	0.8	0.75	0.35					

The simulated S-parameters of the final structure of the proposed filter are shown in **Figure III. 38**. It has an UWB bandpass response (2.9 - 10.6 GHz) with a wide passband of 7.7 GHz, a sharp selectivity, an RL better than 13 dB, and a wide band rejection that exceeds 16 GHz. the dual notches have been created at the desired frequencies 5.8 GHz and 8.0 GHz.

The current distribution of the proposed UWB BPF with dual notched band is illustrated in **Figure III. 39**, at the two notched frequencies 5.8 GHz and 8.0 GHz.

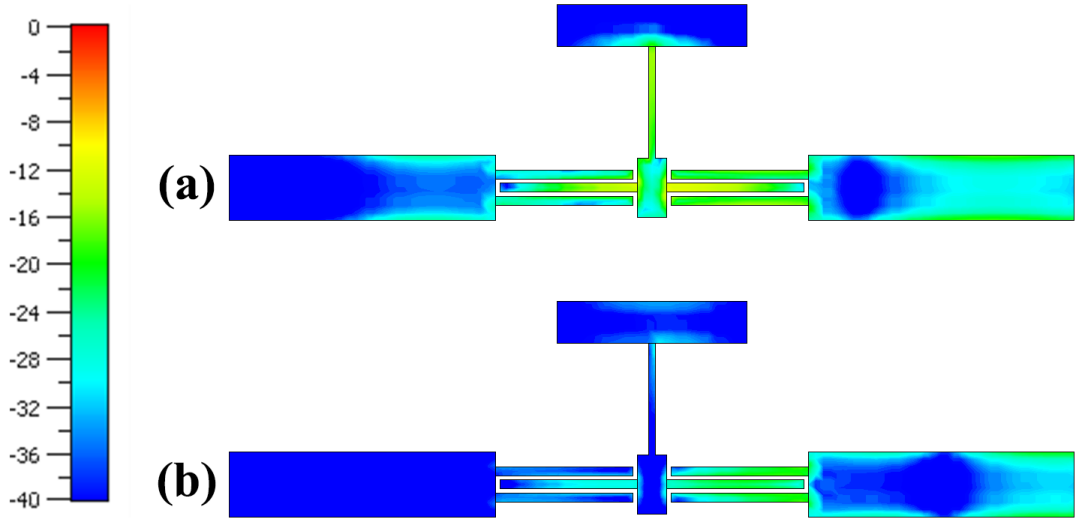

Figure III. 39: Current distribution of the proposed UWB BPF with dual notched bands at a) 5.8 GHz; b) 8.0 GHz

From **Figure III. 39**, It is noticed that the current density is concentrated mainly at the right part of the filter which means that there is no passage of current. As a result, one can say that WiMAX and satellite communication signals have been suppressed by the created notches.

3.4 Fabrication and Measurements

3.4.1 UWB BPF without notches

The proposed UWB BPF without notches is fabricated as illustrated in **Figure III. 40**. The filter occupies a surface of 14.8 mm x 11 mm which demonstrates its compactness.

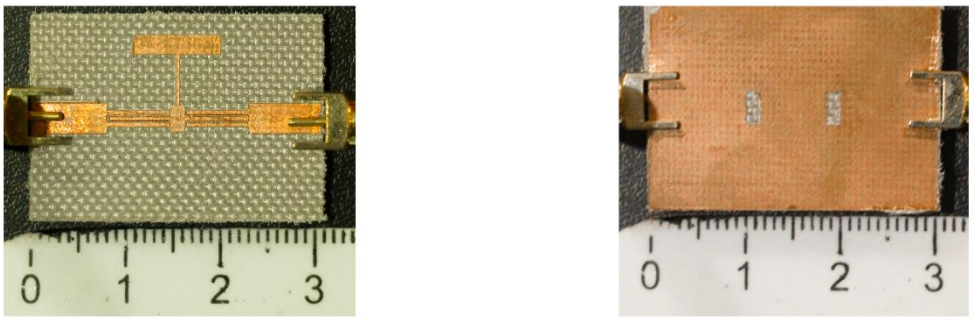

(a) Top view (b) Bottom view

Figure III. 40: Top and Bottom views of the proposed UWB BPF without notches

The filter performance is measured and compared to simulation results as illustrated in **Figure III. 41**.

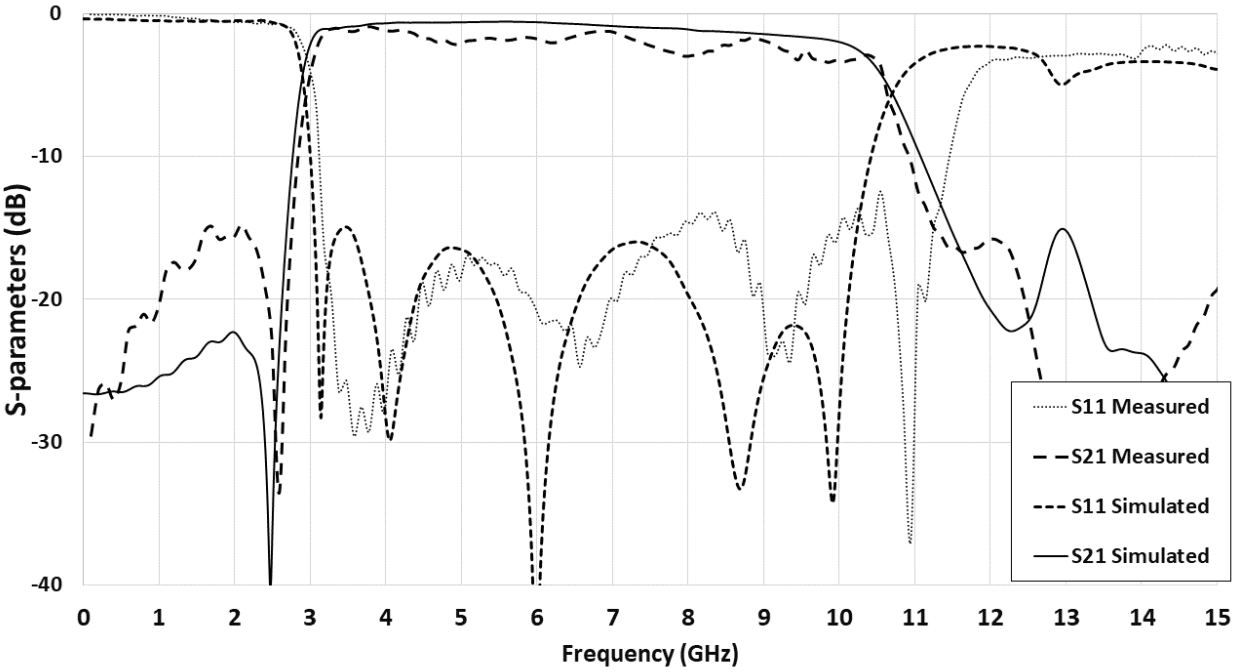

Figure III. 41: S_{11} and S_{21} Simulation and Measurement results of the proposed UWB BPF without notches

As shown in **Figure III. 41**, good agreement between simulation and measurements results is achieved. The measured results possess an ultra-wide impedance bandwidth of 7.7 GHz (2.9 -

10.6 GHz) with a fractional bandwidth of 118.8 %, return loss better than 13 dB, an upper stopband attenuation higher than 15 dB up to 17 GHz, and a sharp selectivity.

Table III. 7 shows comparison between the proposed UWB BPF without notches and some previously reported filters.

Table III. 7: Comparison between the proposed UWB BPF without notches and previously reported filters.

Ref.	h(mm) / ε_r	BW (GHz)	RL (dB)	F_{SB} (GHz)	Size (λ_g^2)
[38]	0.762 / 3.2	7.5	> 9	14	0.41 x 0.36
[39]	1.27 / 2.6	7.27	> 16.5	14.5	2.14 x 0.52
[40]	1.6 / 4.4	5.7	> 11	14.2	2.8 x 0.24
This work	1.62 / 4.3	7.7	> 15	17	1.05 x 0.78

Where F_{SB} is the upper stop band frequency.

Comparing the proposed UWB BPF without notches with other designs is shown in **Table III. 7**. Although this filter is designed using FR-4 commercial substrate which may reduce the bandwidth and impose losses at high frequencies, it still has the largest bandwidth, compact size as compared to [39]. This filter also possesses return loss better than 15 dB and good upper stopband attenuation up to 17 GHz.

3.4.2 UWB BPF with dual notched band

The proposed UWB BPF with double notch is fabricated as illustrated in **Figure III. 42**. The filter occupies a surface of 22.5 mm x 11 mm.

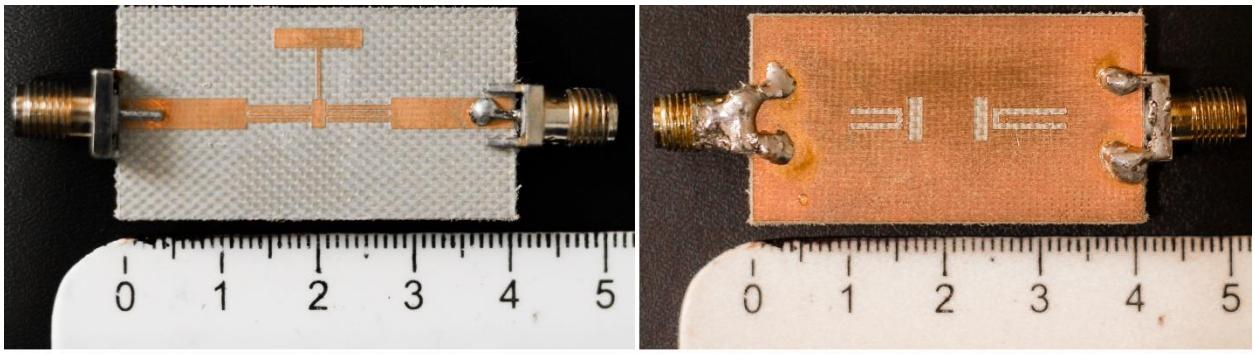

(a) Top view (b) Bottom view

Figure III. 42: Top and Bottom views of the proposed UWB BPF with double notch

The filter performance is measured and compared to simulation results as illustrated in **Figure III. 43** and **Figure III. 44**.

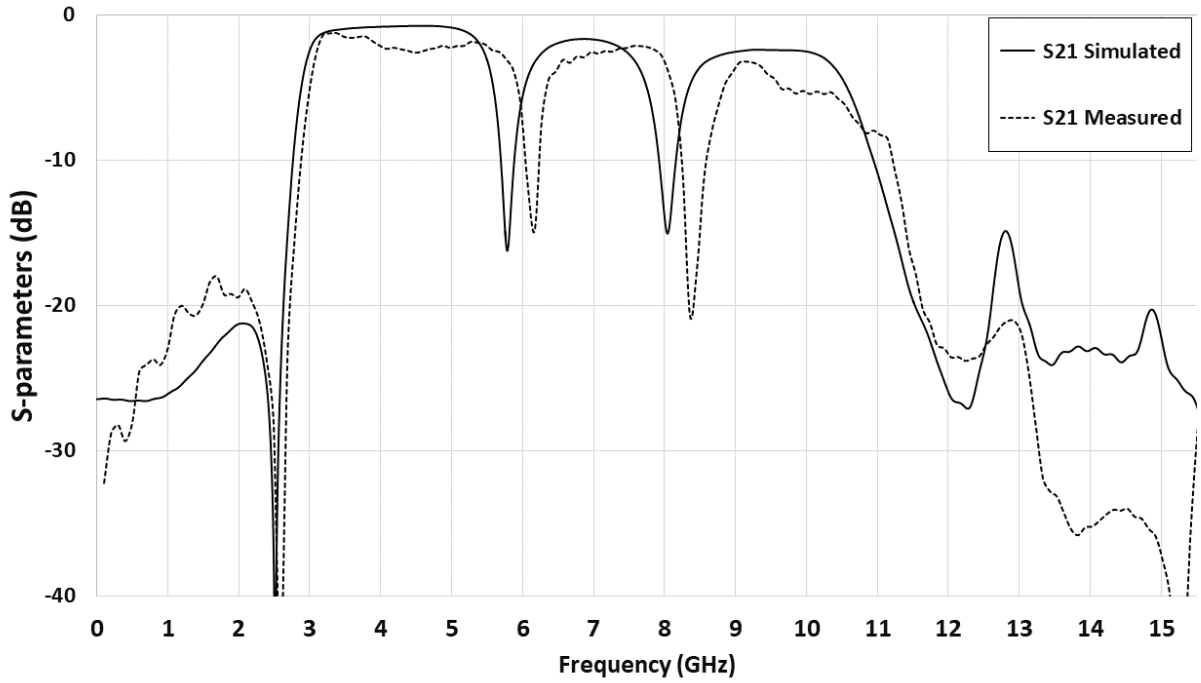

Figure III. 43: S_{21} Simulation and Measurement results of the proposed UWB BPF with double notch

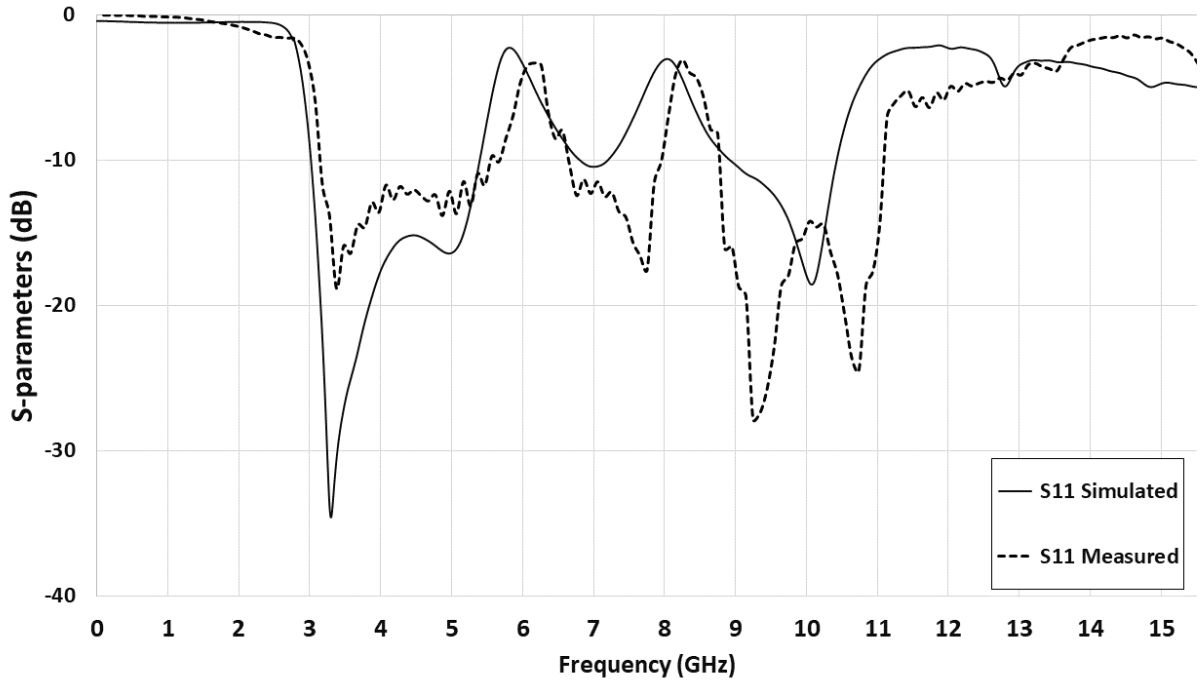

Figure III. 44: S11 Simulation and Measurement results of the proposed UWB BPF with double notch.

As shown in **Figure III. 43** and **Figure III. 44**, good agreement between simulation and measurement results is achieved. The measured results possess an ultra-wide impedance

bandwidth of 7.7 GHz (2.9 - 10.6 GHz) with a fractional bandwidth of 118.8 %, return loss better than 13 dB, an upper stopband attenuation higher than 20 dB up to 16 GHz, and a sharp selectivity. The notched bands have a little shift up (0.35 GHz) compared the simulated results. The notches are created at 6.15 GHz and 8.35 GHz.

Table III. 8: Comparison between the proposed UWB BPF with double notch and previous works.

Ref.	**h(mm) / ε_r**	**BW (GHz)**	**RL (dB)**	**f_{n1} / f_{n2} (GHz)**	**Size (λ_g^2)**
[30]	0.508 / 3.55	7.6	> 9	6.2 / 8.2	0.63 x 1.56
[31]	1.0 / 2.2	7.3	> 13	5.8 / 8.0	1.42 x 0.6
[41]	0.8 / 3.55	8.2	> 10	6.3 / 9.04	1.14 x 0.34
This work	1.62 / 4.3	7.7	> 13	6.15 / 8.35	1.6 x 0.78

Comparing the proposed dual band-notch UWB BPF with previously reported filters is shown in **Table III. 8**. Although this design has the highest substrate thickness which may reduce the spanned range, it still has larger bandwidth as compared to [30]**,** and [31]. This filter also has good performance in terms of return loss which is better than 13 dB.

3.5 Conclusion

In this chapter, a compact ultra-wideband bandpass filter (UWB BPF) with and without dual notched band were designed based on symmetrical structure of a simple uniform line loaded by a stepped-impedance stub (SIS) connected at its center. Two notches were inserted at 5.8 and 8.0 GHz to eliminate WiMAX and satellite communication interferences by embedding two U-shaped slots in the ground plane. The proposed UWB BPF with dual-notch is simulated, fabricated and measured. Satisfactory results were obtained, achieving good performances in terms of ultra-wide impedance bandwidth of 7.7 GHz (2.9 - 10.6 GHz) with a fractional bandwidth of 118.8 %, return loss better than 13 dB, an upper stopband attenuation higher than 20 dB up to 16 GHz, and a sharp selectivity.

General Conclusion

Throughout this project, a compact microstrip UWB BPF with and without dual band-notch was designed, analyzed and fabricated using FR4 substrate material with relative dielectric constant of 4.3, a thickness of 1.62 mm, a copper thickness 0.035 mm and a loss tangent of 0.017. The proposed filter is based on symmetrical structure of a simple uniform line loaded by a stepped-impedance stub (SIS) connected at its center. Two U-shaped DGS units have been introduced to generate notches at 5.8 GHz and 8.0 GHz for WiMAX and satellite communication interferences elimination. The proposed filter consumes a layout area of 1.6 $\lambda_g \times$ 0.78 λ_g. Good performance is obtained in terms of ultra-wide impedance bandwidth of 7.7 GHz (2.9 - 10.6 GHz) with a fractional bandwidth of 118.8 %, return loss better than 13 dB, an upper stopband attenuation higher than 20 dB up to 16 GHz, and a sharp selectivity.

Future work proposal

Further work can be performed to this project stated as follows:

- Creating the equivalent circuit model for the designed filter.
- Implementing quad-notch band by creating another dual notch band to eliminate WLAN interferences at the frequencies 3.5 GHz and 5.0 GHz using open circuited stubs.

References

[1] K. Chang, "RF and Microwave Wireless Systems," John Wiley & Sons, New York, 2000.

[2] K. Chang, I. Bahl and V. Nair, RF and Microwave Circuit and Component Design for Wireless Systems, 2 nd ed., New York: John Wiley & Sons, 2002.

[3] K. M. F. Rabbi, "Miniaturized and Reconfigurable Planar Filters for Ultra-Wideband Applications," WestminsterResearch - PhD thesis,University of Westminster, 2014.

[4] Jia-Sheng Hong and M. J. Lancaster, Microstrip Filters for RF/Microwave Applications, John Wiley & Sons, 2001.

[5] D. M. Pozar, Microwave Engineering, 4th ed., JohnWiley & Sons, 2011.

[6] C. Robinson, B. Souid and T. Piwtorak, "Synthesis and Analysis of Microstrip and Stripline Transmission Line Structures," Final year project report, Syracuse University, 2011.

[7] K. C. Gupta, R. Garg, I. Bahl and P. Bhartia, Microstrip Lines and Slotlines, 2nd ed., Artech House, 1996.

[8] M.-J. Gao, L.S. Wu and J. F. Mao, "Compact notched ultra-wideband bandpass filter with improved out-of-band performance using quasi-electromagnetic bandgap structure," *Progress In Electromagnetics Research,* vol. 125, pp. 137-150, 2012.

[9] T.C. Edward and M.B. Steer, Foundation of interconnect and microstrip design 3rd edition, New York: Wiley, 2000.

[10] A. Azzouz, A. Kachid and A. Benmaache, "Dual-band Microstrip Bandpass Filter Design and Analysis using a DGS Technique," Final year project, IGEE, University of Boumerdes, Boumerdes, 2014.

[11] Bahl and R. Garg, "Characteristics of coupled microstrip lines," *IEEE Transaction on Microwave technology and techniques,* vol. 27, p. 700–705, 1979.

[12] L. Weng, Y. Guo, X.W.Shi and a. X.Q.Chen, "Overview of Defected Ground Structure," *Progress In Electromagnetics Research B,* vol. 7, pp. 173-189, 2008.

[13] M. A. Balalem, Analysis, design, optimization and realization of compact high performance printed RF filter, Master dissertation, Otto-von-Guericke University , 2010.

[14] M. K. Khandelwal, B. K. Kanaujia and a. S. Kumar, "Defected Ground Structure: Fundamentals, Analysis, and Applications in Modern Wireless Trends," *International Journal of Antennas and Propagation,* vol. 20, p. 22, 2017.

[15] Tang, I-Tseng, D.Lin and C.M.Li, "Ultra-Wideband Bandpass Filter Using Hybrid Microstrip Defected Ground Structure," *Microwave and Optical Technology*, vol. 50, no. 12, pp. 3085-3089, 2008.

[16] X. Q. Chen, R. Li, S. J. Shi, Q. Wang, L. Xu and a. X. W. Shi, "A novel low pass filter using elliptic shape defected ground structure," *Progress in Electromagnetics Research B,* vol. 9, pp. 117-126, 2008.

[17] C. Nguyen, Analysis Methods for RF, Microwave, and Millimeter-Wave Planar Transmission Line Structures, New York: John Wiley & Sons, 2003.

[18] N. Benabdallah, N. Benahmed and a. F. T. Bendimerad, "Analysis and Design of an UWB Band pass Filter with Improved Upper Stop band Performances," *International Journal of Modern Engineering Research (IJMER),* vol. 3, no. 2, pp. 1105-1114, 2013.

[19] T. S. Bird, "Definition and Misuse of Return Loss," *IEEE Antennas & Propagation Magazine*, vol. 51, no. 2, pp. 166-167, 2009.

[20] L. Zhu and S. Sun, Microwave Bandpass Filters for Wideband Communications, John Wiley & Sons, 2012.

[21] Z. Chaib and S. Hamrit, "Design and Implementation of an Ultra-Wideband Bandpass Filter with Single/Double Band - Rejection Characteristics," *Final year project report, IGEE, University of Boumerdes, Algeria*, 2017.

[22] R.S.Kshetrimayum, "An introduction to UWB communication systems," *IEEE POTENTIALS,* April 2009.

[23] Z.-C. Hao and J.-S. Hong, "Ultra-Wideband Filter Technologies," *IEEE Microwave Magazine,* vol. 10, pp. 1527-3342, 2010.

[24] L.Zhu, S.Sun and W. Menzel, "Ultra-wideband (UWB) bandpass filters using multiple-mode resonator," *IEEE Microw. Wireless Compon*, vol. 15, no. 11, p. 796–798, 2005.

[25] D.Packiaraj, K. J. Vinoy and A. T. Kalghatgi, "Analysis and design of two layered ultra wide band filter," *Journal of Electromagnetic Waves and Applications*, vol. 23, no. 8-9, p. 1235–1243, 2009.

[26] M.Shobeyri and M. H. Vadjed-Samiei, "Compact ultra-wideband bandpass filter with defected ground structure," *Progress In Electromagnetics Research,* vol. 4, p. 25–31, 2008.

[27] M.N.Jahromi and M. Tayarani, "Miniature planar UWB bandpass filters with circular slot ground," *Progress In Electromagnetics Research Letters,* vol. 3, p. 87–93, 2008.

[28] R.Comez-Garcia and J. I. Alonso, "Systematic method for the exact synthesis of ultra-wideband filtering responses using high-pass and low-pass sections," *IEEE Trans. Microw.Theory Tech.*, vol. 54, no. 10, p. 3751–3764, 2006.

[29] M. Gao, L. Wu and J. F. Mao, "Compact notched ultra-wideband bandpass filter with improved out-of-band performance using quasi-electromagnetic band gap structure," *Progress In Electromagnetics Research,* vol. 125, pp. 137-150, 2012.

[30] O. Mousavi, A. Eskandari and M. Shameli, "Compact UWB Bandpass Filter with Two Notched Bands Using SISLR and DMS Structure," *Progress In Electromagnetics Research M,* vol. 80, p. 193–201, 2019.

[31] H. Peng, Y. Luo and J. Zhao, "Compact Microstrip UWB Bandpass Filter with Two Band-Notches for UWB Applications," *Progress In Electromagnetics Research Letters,* vol. 45, pp. 25-30, 2014.

[32] M. K. Hamood, "Line Thickness for Various Characteristic Impedance of Microstrip Line," *Tikrit Journal of Pure Science,* pp. 140-144, 2013.

[33] H. Shaman and J.-S. Hong, "Asymmetric Parallel-Coupled Lines for Notch Implementation in UWB Filters," *IEEE Microwave and Wireless Components Letters,* vol. 17, no. 7, pp. 516-518, 2007.

[34] L. Zhu, H. Bu and K. Wu, "Aperture compensation technique for innovative design of ultra-broadband microstrip bandpass filter," *IEEE MTT-S Int. Dig.*, vol. 1, p. 315–318, June 2000.

[35] W. Feng, W. Che and Q. Xue., "Compact ultra-wideband bandpass filters with narrow notched bands based on a ring resonator," *IET Microwaves, Antennas & Propagation,* vol. 7, no. 12, p. 961–969, 17 Sept 2013.

[36] S. Mita and S. Ray, "Analysis and Synthesis Of Microstrip Band-Stop Notch Filter Using Hairin DGS," *Depatment of Electonics and Telecommunication Engineering, Jadavpur University*, 2015.

[37] J. Xiao and Y. Zhu, "New U-shaped DGS Bandstop Filters," *Progress In Electromagnetics Research C,* vol. 25, pp. 179-191, 2012.

[38] S. Gupta, M. Kumar and R.Meena, "Design and Analysis of Compact UWB BPF Using Parallel Coupled Microstrip Line With DGS," *Global Journal of Researches in Engineering,* vol. 17, no. 4, pp. 113-122, 2017.

[39] Kavita, S. Kumar and A. Gupta, "Design of UWB Microstrip Filter Using Quarter Wavelength Short Circuited Stubs," *International Journal of Innovative Research in Computer and Communication Engineering*, vol. 2, no. 11, pp. 6736-6742, 2014.

[40] S. Coumar and T. Sadasivam, "Compact Ultra-Wideband BPF Based on Square Resonator Using Inter-digital coupling," *IEEE- Proceeding of Second International conference on Circuits, Controls and Communications*, pp. 218-221, 2017.

[41] S. Nouri, J. Nourinia, C. Ghobadi, F. Alizadeh and B. Mohammadi, "Design and Analysis of Compact BPF with Dual Notch Bbands Based on Stepped-Impedance Resonator for UWB Applications," *Microwave and Optical Technology Letters*, vol. 59, no. 3, pp. 672-674, 2016.

[42] P. Sarkar, R. Ghatak and R. Poddar, "Compact UWB Bandpass Filter With Dual Notch Bands Using Open Circuited Stubs," *IEEE Microwave and Wireless Components Letters*, vol. 22, no. 9, pp. 453-455, 2012.

Appendix A

.

MATLAB program script used in the numerical iteration.

```
f0= 6.85; % Central frequency.
f= [3.1;10.6]; % The two desired transmission zeros.
e=10^-3; % The tolerance.
a=[];
for k=0:0.01:8
    for theta02=0:0.01:pi
        for m=1:2
            theta01(m)=(f0/f(m))
.*atan(1/(k.*tan(theta02.*(f(m)/f0))));% Eq III.11
        end
        if abs(theta01(2)-theta01(1))<e
            W=[k theta01(2) theta02];
            a=[a;W];
        end
    end
end
```

Appendix B

Advanced Design System (ADS)

Advanced Design System (ADS) is an electronic design automation software system produced by Keysight EEsof EDA, a division of Keysight Technologies. It provides an integrated design environment to designers of RF electronic products such as mobile phones, pagers, wireless networks, satellite communications, radar systems, and high-speed data links.

Keysight ADS supports every step of the design process—schematic capture, layout, design rule checking, frequency-domain and time-domain circuit simulation, and electromagnetic field simulation—allowing the engineer to fully characterize and optimize an RF design without changing tools.

Momentum:

Momentum is 3-D planar EM simulation software –integrated in Keysight ADS- for electronics and antenna analysis, a partial differential equation solver of Maxwell's equations based on the method of moments. It is a 3-D planar electromagnetic (EM) simulator used for passive circuit analysis.

It combines full-wave and quasi-static EM solvers to provide insight into EM behavior of MMIC, RFIC, RF Board, Signal Integrity, filters, and antenna designs.

LineCalc:

LineCalc is an analysis and synthesis program for calculating electrical and physical parameters of single and coupled transmission lines.

LineCalc can communicate directly with the circuit simulators. A parameter data for selected circuit design elements, can be sent along with data on any associated substrates or walls, directly from the simulator to LineCalc. After the element parameter values are calculated, the associated schematic or layout circuit design in the active simulator can be updated immediately with the LineCalc results.

CST Microwave Studio:

CST MICROWAVE STUDIO **(CST MWS)** is a powerful tool for the 3D electromagnetic (EM) simulation of high frequency components. CST MWS offers unparalleled performance, making it first choice in technology leading R&D departments.

CST MWS enables the fast and accurate analysis of high frequency (HF) devices such as antennas, filters, couplers, planar and multi-layer structures and SI and EMC effects. Exceptionally user friendly, CST MWS quickly gives an insight into the EM behavior of high frequency designs.

Choice of Solver Modules

Users of CST MWS can choose between six powerful solver modules each offering distinct advantages in their own domains. In the CST Complete Technology approach, the seamless integration of these solvers in one user interface enables the easy selection of the most appropriate solver for a given problem class, delivering improved simulation performance and unprecedented simulation reliability through cross verification.

Workflow Integration

A wide range of import/export filters enable the easy exchange of geometrical data with CAD tools. Furthermore, imported structures can be modified, parameterized, and used for optimization and design studies. Special interfaces to various EDA tools for signal integrity analysis and to RF circuit/system simulators for EM/circuit co-simulation enhance and unite the capabilities of different worlds.